Characteristics of Multi-h Coded Modulation

by

Brian P. Crawford

B.S. Engineering *Arizona State University*

Submitted to the Department of Electrical Engineering
in partial fulfillment of the requirements for the degree of

Master of Science in Electrical Engineering

at the

UNIVERSITY OF CAPE TOWN

June 1994

Signature of Author .....
Department of Electrical Engineering
February 7, 1994

Certified by .....
Dr. Robin M. Braun
Director of the Communications Research Group
Thesis Supervisor

Accepted by .....
Prof. Barry J. Downing
Head of Department

1 Acknowledgments

The overwhelming support for this work by Dr. Robin M. Braun is greatfully appreciated. Assistance in the review of these results by colleagues of the Communications Research and Small Aperture Radar Groups is acknowledged. The project support of Plessey-Tellumat is appreciated.

Contents

List of Figures

Abstract

Multi-h Coded Continuous-Phase Frequency Shift Keying (Multi-h CPFSK) has gained interest in recent years because it offers an additional degree of freedom in the coding of CPFSK. Similar to Trellis Coded Modulation (TCM), it does not use redundancy to achieve coding gain. Hence with properly chosen modulation indices, impact to spectral occupancy is kept to a minimum.

While there has been less attention given of this method as compared with TCM, this method can also be used with data coding. In cases where data coding is to be implemented, simultaneous use of Multi-h coding can be implemented with very little increase in complexity.

In this thesis, a thorough mathematical review of this technique is made. A multi-oscillator multi-h coded modulator is shown similar to one presented by Massey for MSK. A unique analytical tool called a multi-oscillator trellis is presented. This considers the phase transitions with respect to each of the signalling frequencies instead of the center frequency, f_o. The multi-oscillator trellis is used to determine the state machine that will switch a bank of oscillators. The purpose of the state machine is to maintain continuous phase at the multi-oscillator output while generating the proper signal frequencies according to the data and modulation index.

The Maximum Likelihood Detection process at the receiver is shown as a partition of an uncoded CPFSK signal. Finally, an analysis is made to determine if a modulator with a non-linear frequency-voltage characteristic is suitable in a coherent multi-h coded application.

Much of the literature on this topic has been comparative to PSK. It is the intent of this work to use FSK and MSK as the baseline to determine how existing structures may be extended to realize the benefits of multi-h coding. The application of this coding to an 8 Mbps 23 GHz CPFSK point-to-point terrestrial communications system is also a topic of this thesis. It is in this context that the analysis is made.

2 Introduction

Frequency Shift Keying (FSK) has become a useful mode of communication when the transmitter or channel have non-linear characteristics. To minimize power consumption of transmission systems requiring greater transmitter power, higher efficiency Class C amplifiers are desirable. Simplifications to transmitter and receiver structures can also be made when signal linearity is not of significant importance. These applications require a modulation format that survive distortion of such stages. FSK and PSK have this characteristic.

In general, FSK is not as spectrally efficient as Amplitude-Shift (ASK) or Phase-Shift Keying (PSK). ASK and PSK show remarkable increase in spectral efficiency with greater number of signaling levels, but suffer a corresponding decrease in bit-error performance and sensitivity to channel and transceiver non-linearities. This is especially true at higher orders of signaling. At least for a moderate number of signaling levels, PSK shows an even greater amount of spectral efficiency at the cost of bit-error performance [1]. FSK, on the other hand, experiences bit-error improvement for increases in signal levels. It also shows a greater integrity through non-linear channels and noise.

2.1 Definition and Motivation of Continuous-Phase FSK.

With any type of modulation, more efficient means of transmission are desirable. Among the refinements to the bit-error rate and spectral performance of FSK which have been made, Continuous-Phase FSK (CPFSK) has proved to have a significant decrease in bandwidth. In addition to the frequency shifted information signal, the following constraint is placed on the signal phase:

$$\phi(t,\alpha) = 2\pi \sum_{i=-\infty}^{+\infty} h_i \alpha_i q(t - iT_s). \tag{1}$$

where $h = \{h_i\}$ is the modulation index (constant in the uncoded case), $\bar{\alpha} = \{\alpha_i\}$ is the M-ary transmitted data vector, and $q(t)$ is the phase response:

$$q(t) = \int_{-\infty}^{t} g(\tau) d\tau.$$

$g(\tau)$ is defined as the instantaneous frequency pulse function. This expression describes the shape of the pulse. For a simple rectangular pulse, g(t) is constant and equal to $\frac{1}{2T_s}$ corresponding to a linear slope between symbol-boundaries.

The merit of this constraint may be seen by a comparison of the power spectral density expression for CPFSK (e.g. Fast-Frequency Shift Keying, Minimum Shift Keying, etc.) with that of non-

continuous FSK [2]. Without the continuous-phase constraint, FSK can be described as:

$$s(t) = \begin{cases} \sqrt{\frac{2E_b}{T_b}} cos\left[2\pi\left(f_c + \frac{\Delta f}{2}\right)t + \theta_1\right] & \text{for symbol 1,} \\ \sqrt{\frac{2E_b}{T_b}} cos\left[2\pi\left(f_c - \frac{\Delta f}{2}\right)t + \theta_2\right] & \text{for symbol 0.} \end{cases}$$

where θ_1 and θ_2 are two random variables of phase distributed independently over the interval $(0, 2\pi)$. The resulting signal is described as the sum of these two On-Off Keyed sinusoidal sources. The Power Spectral Density of an On-Off Keyed line code is:

$$S_{x1} = \sqrt{\frac{E_b}{2T_s}}\delta(f) + \frac{E_b}{2} sinc^2(fT_b).$$

Since in the binary case each waveform is equally likely, half the power is contained in each modulated waveform for symbol 0 and 1. Determining the power spectral density of each waveform after modulation can be found by the autocorrelation method. Because the statistically independent phases θ_0 and θ_1 must be taken into account over the domain (0,2π) [2], the derivation is arduous. The result is :

$$\begin{aligned} S_1(f) &= \frac{E_b}{8T_b}\left[\delta\left(f + f_c + \frac{\Delta f}{2}\right) + \delta\left(f - f_c - \frac{\Delta f}{2}\right)\right] \\ &\quad + \frac{E_b}{8}\left\{sinc^2\left[T_b\left(f + f_c + \frac{\delta f}{2}\right)\right] + sinc^2\left[T_b\left(f - f_c - \frac{\delta f}{2}\right)\right]\right\}, \qquad (2) \\ S_2(f) &= \frac{E_b}{8T_b}\left[\delta\left(f + f_c - \frac{\Delta f}{2}\right) + \delta\left(f - f_c + \frac{\Delta f}{2}\right)\right] \\ &\quad + \frac{E_b}{8}\left\{sinc^2\left[T_b\left(f + f_c - \frac{\delta f}{2}\right)\right] + sinc^2\left[T_b\left(f - f_c + \frac{\delta f}{2}\right)\right]\right\}. \qquad (3) \\ &\quad 0 \le t \le T_b \end{aligned}$$

If it is assumed that $f_c \gg \Delta f$, then the PSD falls off as the inverse square of frequency since sinc(x) decreases according to $\frac{1}{|x|}$ [3].

For the continuous case, the FSK signal is described by polar frequency shifts of a single oscillator:

$$s(t) \;=\; \sqrt{\frac{2E_b}{T_b}} cos\left(2\pi f_c t \pm \frac{\pi t}{T_b}\right), \quad 0 \le t \le T_b$$

This may be expanded to:

$$s(t) = \sqrt{\frac{2E_b}{T_b}} cos\left(\frac{\pi t}{T_b}\right) cos\left(2\pi f_c t\right) \mp \sqrt{\frac{2E_b}{T_b}} sin\left(\frac{\pi t}{T_b}\right) sin\left(2\pi f_c t\right). \qquad (4)$$

The PSD of a polar line code is simply:

$$S(f) = \frac{\Psi_g(f)}{T_b},$$

where $\Psi_g(f)$ is the PSD of the symbol shaping function.

The expanded expression for s(t) in equation 4 may be interpreted as sinusoidal shaped pulses of frequency $\frac{1}{2T_b}$ modulated in-phase and quadrature at f_c Hz. The PSD of the first term is constant, independent of the information, and equal to two delta functions of weight $\frac{E_b}{2T_b}$ of frequency $\pm\frac{1}{2T_b}$. The second term, a sinusoidal pulse $\sqrt{\frac{2E_b}{T_b}}sin(\frac{\pi t}{T_b})$ defined only over the interval $0 \leq t \leq T_b$. The pulse is positive for symbol 1 and negative for symbol 0. The energy spectral density of this function is:

$$\begin{aligned}
\Psi_g(f) &= \frac{1}{\pi}\int_0^{\infty} |F(\omega)|^2 d\omega \\
&= \frac{1}{\pi}\int_0^{T_b} |\sqrt{\frac{2E_b}{T_b}} sin\left(\frac{\pi t}{T_b}\right)|^2 d\omega. \\
&= \frac{8E_bT_bcos^2(\pi T_b f)}{\pi^2(4T_b^2f^2-1)^2}.
\end{aligned}$$

As can be seen, this PSD falls off as a function of f^4 [3].

When the constant-envelope forms of modulation are desired for use in a non-linear or noisy channel, coding can also be used for an improvement in the bit-error rate performance similar to that employed in PSK or QAM. The improvement is obtained by designing into the structure an inherent ability at the receiver to detect and correct a limited number of errors, thereby decreasing the overall error rate. In the case of data coding, however, additional bandwidth is required. The intent of bit-error rate improvement is to achieve the theoretical limits on channel capacity specified by Shannon more closely [4].

As can be seen by the expression for $\phi(t,\alpha)$, the phase of the current CPFSK signal possesses memory in the phase component since it is cumulative. DeBuda showed this accumulated phase may be used to an advantage in improving the bit-error performance when decisions at the receiver are made based on signal observations of more than one symbol-period [5].

Multi-h is one method of coded modulation. This form of coding uses one of K different modulation indices, sequentially, for each symbol-period. In it's simplest form, the modulation indices used repeat in sequence among a discrete finite set, $H_k = \{h_1, h_2, \ldots, h_k\}$. The set is repeated every K symbols. Upon examination of the equation 1, it is seen that multi-h methods offer an additional degree of freedom of coding to methods of data ($\bar{\alpha}$) coding.

Like Trellis-Coded Modulation, Multi-h coding does not use data redundancy to achieve coding gain [6]. This requires an increase in implementation complexity, however. As will be shown, this

increase in complexity is manifest in the standard optimum receiver by the addition of frequencies (i.e. points in signal space) which must be resolved. Because the coding is achieved using a variation of the modulation index, the spectrum is also effected. Proper selection of the set of indices, however, can minimize any increase in spectral occupation and complexity in implementation.

In much of the subject literature, performance comparisons are with respect to PSK. The scope of this thesis will be to show the unique characteristics of CPFSK with Multi-h coding in comparison to uncoded binary CPFSK. Receiver and transmitter structures used for this scheme will be analyzed. Finally, a study of the combined effect of coded CPFSK on non-linear modulators in a noisy channel will be made.

3 Mathematics of Multiple Modulation Index Modulation

3.1 Euclidean Distance Improvements by Multi-h Coding

The motivation for varying the modulation index to achieve performance improvement can be seen by examination of the minimum possible Euclidean distance for the transmitted signal sequence. In Maximum Likelihood Signal Detection, the squared Euclidean distance is determined between any two CPFSK signals $s(t,\bar{\alpha})$ and $s(t,\bar{\beta})$ corresponding to two symbol sequences which separate at a symbol-boundary at $t = 0$, and then *merge* at the symbol-boundary of a later time $t = iT_s$ to a common phase. The Euclidean distance between any two signals for any length of time is:

$$D^2 = \sum_{i=0}^{n-1} \int_{iT_s}^{(i+1)T_s} [s(t,\bar{\alpha}) - s(t,\bar{\beta})]^2 dt$$

The earliest possible merge of any possible pair of signals is considered to be the minimum distance for which this calculation is made. When the carrier frequency is considered to be much greater than the signaling frequency, with use of trigonometric identities the expression becomes:

$$D^2 = \frac{2E_s}{T_s} \sum_{i=0}^{n-1} \int_{iT_s}^{(i+1)T_s} (1 - cos[\phi(t,\bar{\alpha}) - \phi(t,\bar{\beta})])dt.$$

where n is the number of symbol-periods for which signal observation is assumed. This expression is normalized with respect to the symbol energy for M-ary signaling for $M > 2$ by:

$$d^2 = \frac{D^2}{2E_b}$$

where

$$E_b = \frac{E_s}{log_2 M}$$

The distance d^2 accumulates for each symbol-period, and depends on the phase difference $\phi(t,\bar{\alpha}) - \phi(t,\bar{\beta})$. The earliest possible merge of any possible pair of signals is considered the minimum distance, d_{min} and is a fundamental characteristic of coding. By examination of equation 1, it is seen that minimum distance considerations are made using only the accumulated phase. The coding properties of multi-h are examined in this manner as well.

3.2 Phase Trellis Representation of CPFSK.

A *phase trellis* is the graphical expression of the instantaneous phase (equation 1) for all possible data sequences, and is an important tool in the analysis of CPFSK. The modulation index, h_i, predicts the magnitude of the slope of the phase path. The data vector, $\bar{\alpha}$, predicts the sign of the slope. The path course between symbol-boundaries on the trellis is determined by the instantaneous frequency pulse function, $g(t)$. Recalling that the derivative of phase is frequency, the slope of the trellis path is proportional to the signal frequency.

For CPFSK formats, coding and even spectral improvements are manifest in the CPFSK trellis path in various ways. Coding is used to maximize d^2_{min}. In terms of the phase trellis, the intent is to delay the earliest merge of any two paths. This corresponds directly with the minimum Euclidean distance criteria. The least number of intervals over which any two signal paths can merge is called the constraint length, C [7]. Mathematically, basic multi-h coding is used to increase the number of intervals over which the summation of D^2 is made. Multi-h increases this constraint length by using each element of a finite, discrete set of K modulation indices sequentially over K symbol-periods.

3.3 Signal State Representation

The phase states at the symbol-boundary are a function of the accumulated phase. The most basic form of this coding uses rational indices of common denominator:

$$H_K = \{h_1, h_2, ..., h_K\} = \left\{ \frac{p_1}{q}, \frac{p_2}{q}, \ldots, \frac{p_K}{q} \right\}$$

where q and p are integers and h are multiples of $\frac{1}{q}$. Any set H_K consisting of only rational indices has the inherent property that all phases at times iT are a multiple of $\frac{2\pi}{q}$. Therefore, only a finite number of modula-2π phase states exist for the set. This simplifies the requirement for detection and decoding at the receiver.

There are qKM signal states, (θ, i), in the coded waveform where θ progresses over q phases and i over K times for each of the M signal levels. An important characteristic of multi-h coding is the difference between signal states and phase states. By examination of a phase trellis representation of a multi-h coded signal, it is seen that all qKM signal states are not necessarily at every symbol interval. It is also apparent that for M-ary signaling where $M > 2$, a particular phase state may exist for more than one level of signaling. This does not occur for "good" codes. The number of phase states, then, is $\leq$ the number of signal states. This can be used to simplify the implemented structure. For a set H_K, let:

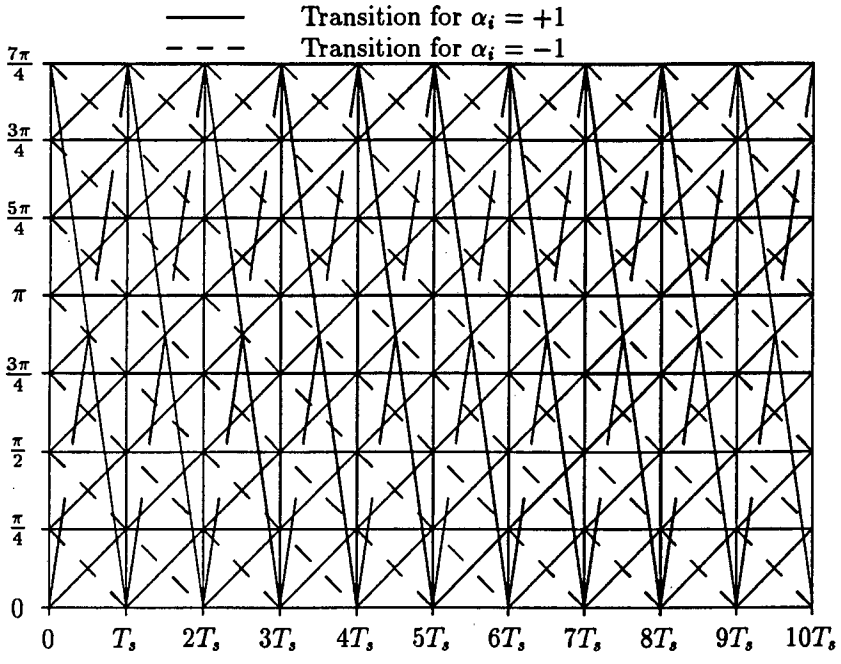

Figure 1: Uncoded CPFSK Trellis for $h_1 = \frac{1}{4}$.

$$\Gamma = \sum_{i=1}^{K} p_i$$

The number of phase states in the trellis is q if Γ is even and 2q if Γ is odd, and the period of the trellis is K if Γ is even and 2K if Γ is odd. Since a merge in the state trellis corresponds to a merge in the phase trellis. The distance calculations are often discussed in terms of the more intuitive phase trellis.

3.4 Phase Trellis Representation of Multi-h Coded CPFSK

The trellis for a multi-h coded signal using the set $H_2 = \{\frac{2}{4}, \frac{3}{4}\}$ is shown in figure 4. A separate uncoded trellis for each index is shown in figures 1 and 2. The coded trellis may be interpreted as a superposition of the uncoded trellises of each index.

The trellis diagram of a coded CPFSK signal is also shown in figures 4 and 5 for two 2-H sets $H_2 = \{\frac{2}{4}, \frac{3}{4}\}$, $H_2 = \{\frac{1}{4}, \frac{3}{4}\}$. A trellis for a 3-H set $H_3 = \{\frac{4}{8}, \frac{5}{8}, \frac{6}{8}\}$ is shown in figure 6. Each state in the diagram denotes a phase state at a symbol boundary.

Upon examination of the path of shortest merge in figure 4, it can be seen that a multi-h code of constraint length C must occupy at least 2^K different phase states at the symbol-intervals [7]. A result is the constraint length, C, is no longer than K+1 symbol-periods and also depends on q. While $C \leq K + 1$ for all H_K, there exist proper modulation index sets H_K which achieve the maximum

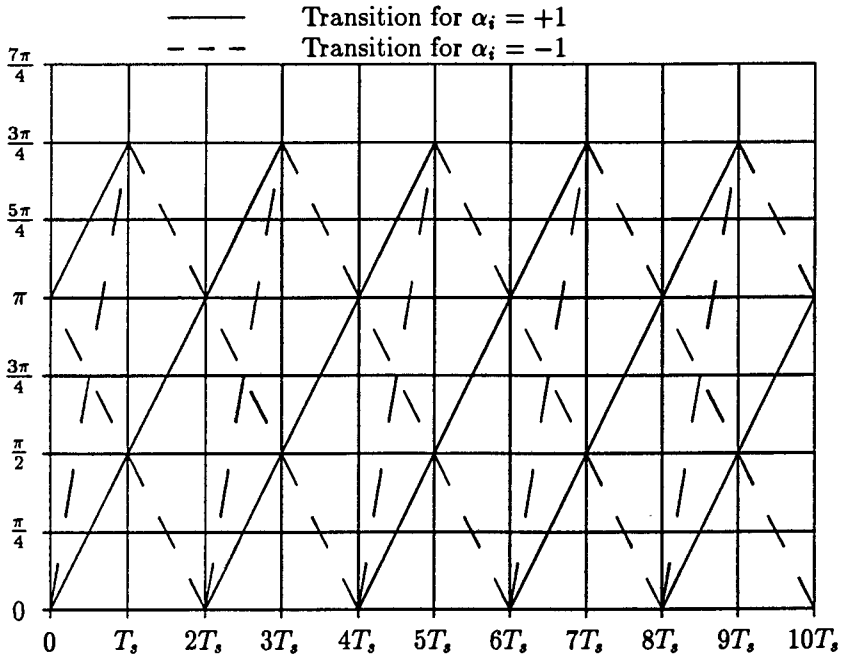

Figure 2: Uncoded CPFSK Trellis for $h_2 = \frac{2}{4}$.

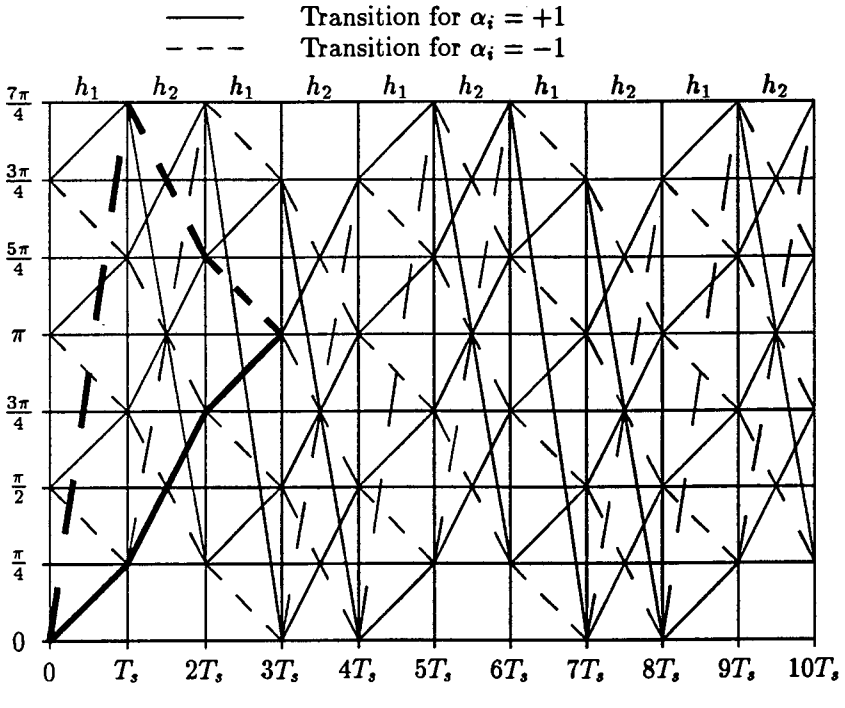

Figure 3: Coded CPFSK Trellis for $H_2 = \{\frac{1}{4}, \frac{2}{4}\}$.

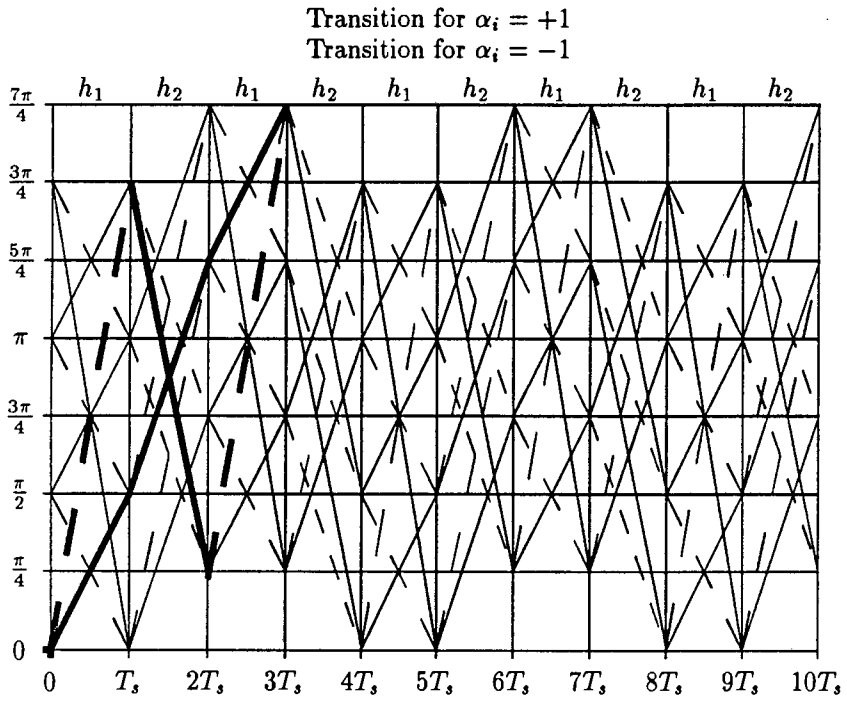

Figure 4: $H_2 = \{\frac{2}{4}, \frac{3}{4}\}$.

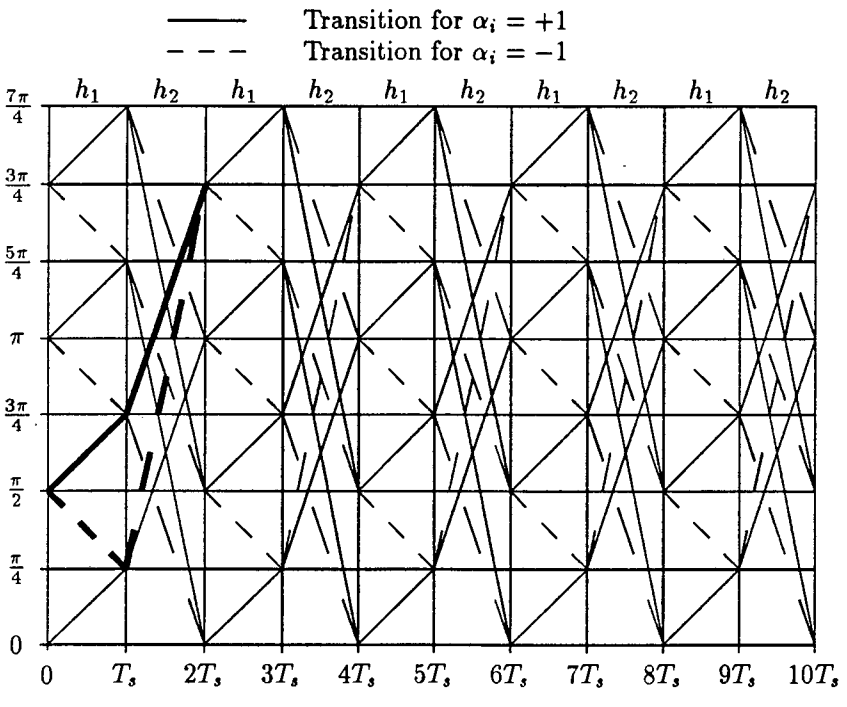

Figure 5: $H_2 = \{\frac{1}{4}, \frac{3}{4}\}$.

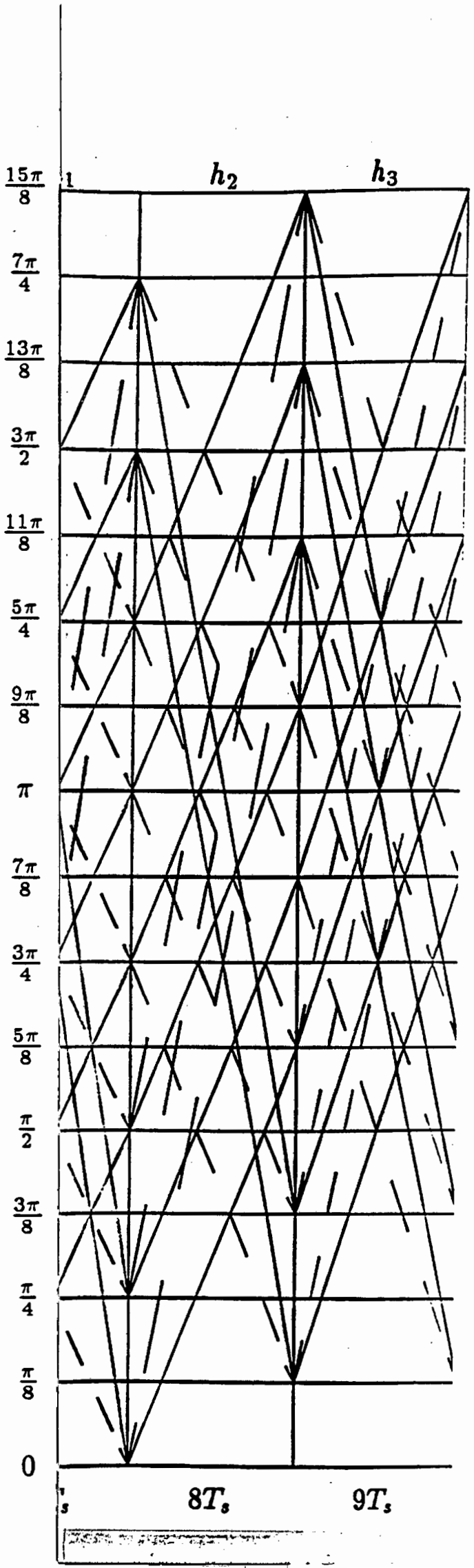
$\frac{15\pi}{8}$
$\frac{7\pi}{4}$
$\frac{13\pi}{8}$
$\frac{3\pi}{2}$
$\frac{11\pi}{8}$
$\frac{5\pi}{4}$
$\frac{9\pi}{8}$
π
$\frac{7\pi}{8}$
$\frac{3\pi}{4}$
$\frac{5\pi}{8}$
$\frac{\pi}{2}$
$\frac{3\pi}{8}$
$\frac{\pi}{4}$
$\frac{\pi}{8}$
0
1
h_2
h_3
$8T_s$
$9T_s$

attainable constraint length of $K+1$, provided $q \geq M^K$. With any coding method, a "good code" which achieves this maximum performance is desired. This criteria is met with multi-h by the selection of the set H_K. This consideration is merely an arithmetic one.

It can be seen by the corresponding trellis shown previously that the constraint length for $H_2 = \{\frac{1}{4}, \frac{2}{4}\}$ is $C = 3$. Figure 5 indicates a premature merge after only two symbol-periods for the set $H_2 = \{\frac{1}{4}, \frac{3}{4}\}$. According to equation 5, the minimum distance d_{min} in the $\{\frac{1}{4}, \frac{2}{4}\}$ case is calculated using two signal paths through the trellis corresponding to data sequences {-1,-1,-1} and {+1,+1,+1} as shown in figure 3. For each data vector, $\bar{\alpha}$ and $\bar{\beta}$, the corresponding phase equation in each interval (i = 1, 2, 3) is:

$$\begin{aligned}
\phi_{\alpha 1} &= -\frac{\pi}{4}\frac{t}{T_s} \\
\phi_{\alpha 2} &= -\frac{\pi}{4} - \frac{\pi}{2}\frac{t}{T_s} \\
\phi_{\alpha 3} &= +\frac{5\pi}{4} - \frac{\pi}{4}\frac{t}{T_s} \\
\phi_{\beta 1} &= +\frac{\pi}{4}\frac{t}{T_s} \\
\phi_{\beta 2} &= +\frac{\pi}{4} - \frac{\pi}{2}\frac{t}{T_s} \\
\phi_{\beta 3} &= +\frac{3\pi}{4} - \frac{\pi}{4}\frac{t}{T_s}
\end{aligned}$$

Applying these expressions of ϕ to equation 5, the result is:

$$\begin{aligned}
D^2_{min} &= \frac{2E_s}{T_s}\sum_{2}^{i=0}\int_{iT_s}^{(i+1)T_s}\left\{1 - cos[\phi(t,\bar{\alpha}) - \phi(t,\bar{\beta})]\right\}dt \\
&= \int_0^{T_s}\left\{1 - cos\left[\left(-\frac{\pi}{4}\frac{t}{T_s}\right) - \left(\frac{\pi}{4}\frac{t}{T_s}\right)\right]\right\}dt \\
&\quad + \int_{T_s}^{2T_s}\left\{1 - cos\left[\left(\frac{\pi}{4} + \frac{\pi}{2}\frac{t}{T_s}\right) - \left(-\frac{\pi}{4} - \frac{\pi}{2}\frac{t}{T_s}\right)\right]\right\}dt \\
&\quad + \int_{2T_s}^{3T_s}\left\{1 - cos\left[\left(\frac{3\pi}{4} + \frac{\pi}{4}\frac{t}{T_s}\right) - \left(\frac{5\pi}{4} - \frac{\pi}{4}\frac{t}{T_s}\right)\right]\right\}dt \\
&\quad \text{with the use of trigonometric identities, these expressions simplify to:} \\
&= \int_0^{T_s}\left[1 - cos\left(\frac{\pi}{2}\frac{t}{T_s}\right)\right]dt \\
&\quad + \int_{T_s}^{2T_s}\left[1 - sin\left(\pi\frac{t}{T_s}\right)\right]dt \\
&\quad + \int_{2T_s}^{3T_s}\left[1 - sin\left(\frac{\pi}{2}\frac{t}{T_s}\right)\right]dt \\
&= T_s\left(3 + \frac{2}{\pi}\right)
\end{aligned}$$

Since $d^2_{min} = \frac{D^2_{min}}{2E_b}$, it follows that $d^2_{min} = 3.6366$. For the set $\{\frac{1}{4}, \frac{3}{4}\}$, however, a very similar calculation shows $d^2_{min} = 2$, which is the same minimum distance as that for MSK. Nothing would be gained by implementing this latter code set.

3.5 The Selection of Multi-h Code Sets

Research was conducted through current literature for a simple mathematical expression which determined a general set H_K with a constraint length of $K+1$. Due to the nature of all of the applicable criteria cited thus far, a general algorithm is the simplest form available. Premji presented such a novel method for the determination of H_K sets which maximize the constraint length [8]. The following steps are presented in terms of the phase difference expression of d^2_{min}. Constraints are placed on the beginning and ending phases of the summation of equation 1.

For $h_1 = \frac{p_1}{q_1}$, choose p_1 such that any two paths through the trellis which both leave the same node at $t = 0$ do not merge at the same mod-2π phase state at a later time $t = iT$, for any i. If for any two trellis paths, the phase state at the merging symbol-boundary is:

$$m_1 \pi \frac{p_1}{q} - m_2 \pi \frac{p_1}{q} \qquad m_1, m_2 \in \{\pm 1, \pm 3, ..., \pm(M-1)\}, \quad m_1 \neq m_2, \tag{5}$$

then the constraint for p_1 may be expressed mathematically:

$$p_1 \neq \frac{nq}{\Delta}, \qquad \Delta = \frac{m_1 - m_2}{2} \in \{\pm 1, \pm 2, ..., \pm(M-1)\} \tag{6a}$$

n any integer.

Assuming p_1 has been chosen as described by equation 6a, p_2 follows the same constraint as p_1, $p_2 \neq p_1$, and should also be chosen such that the total phase difference between terminating nodes is a non-integer product of 2π:

$$\Delta_1 2\pi \frac{p_1}{q} + \Delta_2 2\pi \frac{p_2}{q} \neq n2\pi$$

In similar form the mathematical constraints for p_2 are:

$$p_2 \neq \frac{nq}{\Delta}, \tag{6b}$$

$$\neq \frac{nq - \Delta_1 p_1}{\Delta_2}.$$

$$\Delta, \Delta_1, \Delta_2 \in \{\pm 1, \pm 2, ..., \pm(M-1)\}$$

Given that p_1 and p_2 are chosen in accordance with equation 6a and equation 6b, p_3 must also satisfy the conditions specified for p_1 and p_2, and remain at non-integer multiples of 2π:

$$\Delta_1 p_1 + \Delta_2 p_2 + \Delta_3 p_3 \neq nq,$$

so that:

$$\begin{aligned} p_3 &\neq \frac{nq}{\Delta}, \\ &\neq \frac{(nq - \Delta_1 p_1)}{\Delta_3} \\ &\neq \frac{nq - \Delta_2 p_2}{\Delta_3} \\ &\neq \frac{nq - \Delta_1 p_1 - \Delta_2 p_2}{\Delta_3} \\ &\Delta, \Delta_1, \Delta_2, \Delta_3 \in \{\pm 1, \pm 2, ..., \pm(M-1)\} \\ &\text{n is any integer.} \end{aligned} \tag{6c}$$

The general form of these constraints is:

choose $p_1, p_2, ..., p_{K-1}$ in that order so that the i^{th} value satisfies:

$$p_i \neq \frac{|nq - \Delta_{i-1} p_{i-1} - \Delta_{i-2} p_{i-2} - ... - \Delta_2 p_2 - \Delta_1 p_1|}{\Delta}. \tag{6}$$

where:

$p_1, p_1, ..., p_{i-1}$ are known,

$\Delta_j = 0, \pm 1, \pm 2, ..., \pm(M-1)$for j=0, 1,....,i-1

$\Delta = 1, 2, ..., (M-1)$,

and n is any integer.

For example, let q=8 and M=2 in order to select a H_3 set. Then, for any two trellis paths, the phase state at the merging symbol-boundary according to equation 5 must be: $\pm\pi\frac{p_1}{8} \mp \pi\frac{p_1}{8}$, or $p_1 \neq \frac{8n}{\pm 1}$ where n is any integer. Not only is this a constraint due to coding reasons but it will be shown that $p_1 = \frac{8n}{\pm 1}$ or $h_1 = n$ cause undesirable spectral components. In this example, let $p_1 = 4$.

For p_2 the same constraint for p_1 applies. In order that the total phase difference between the

path of two terminating phase states be a non-integer multiple of 2π and taking into account p_1, the phase difference is $\pm 2\pi\frac{4}{8} \mp 2\pi\frac{p_2}{8} \neq n2\pi$, where n is any integer and $\Delta_1, \Delta \in \{\pm 1, \pm 2, \ldots, \pm(M-1)\}$. The new constraint for p_2 is $p_2 \neq \frac{8n \mp 4}{\mp 1}$, or $8n \pm 4$. p_2 is chosen to be 5.

Finally, for p_3 the requirement $\pm 4 \pm 5 \pm p_3 \neq 8n$ yields the constraints:

$$\begin{aligned} p_3 &\neq \frac{8n}{\pm 1} = 8, \\ &\neq \frac{8n - \pm 4}{\pm 1} = 4, \\ &\neq \frac{8n - \pm 5}{\pm 1} = 3, \\ &\neq \frac{8n - \pm 4 - \pm 5}{\pm} = 1, \\ &\Delta, \Delta_1, \Delta_2, \Delta_3 \in \{\pm 1\}. \end{aligned}$$

This exercise results with the set $H_3 = \{\frac{2}{8}, \frac{4}{8}, \frac{5}{8}\}$, $\{\frac{4}{8}, \frac{5}{8}, \frac{6}{8}\}$, or $\{\frac{4}{8}, \frac{5}{8}, \frac{7}{8}\}$.

3.6 Non-linear Multi-h Coding

Other similar methods have been presented for additional coding gains by further delay of the first merge on the phase-trellis. Fonseka suggests a method quite similar to multi-h called non-linear coding [9]. By non-linear coding it is meant that instead of using the set of H_K sequentially, the order of the indices used from the set is dependent on both the transmitted symbol and the present state of the system. Specifically, the index used in a particular symbol-period depends on the current symbol, the previous $L-1$ symbols, and on the current phase state. This form leads to simple criteria for maintaining the constraint length to it's upper bound, which is a function of K. As an alternative to the phase-state trellis given previously, a state transition matrix T_N and $L_{N,n}$ is defined. The state transition matrix consists of only 1 or 0, where a 1 represents the existence of a path and a 0 represents the absence. The state location matrix is defined at the end of a symbol-interval. $L_{N,n}$ is of dimension N X N and equal to the number of paths terminating at each state in existence at the end of a particular symbol-interval.

Note that for non-linear multi-h coding, *any* index from the set could be used in a symbol-period. It is possible, for example, for a particular index to be used consecutively. Because the computational complexity of the code grows exponentially with M and L, this method is requires a more complex structure to implement in general. If the set (θ, i) is considered as a state model whose structure is unique for different H_K, it is intuitive that the total number of states is important in the determination of the transmitter and receiver structure. Another criteria of a optimum set H_K, then, is that it possess the minimal number of signal or phase states for which the minimum distance is maximized. This is a fundamental trade-off in implementation.

The path through the trellis is determined by equation 1. The phase states at the symbol-boundaries are determined by h_i and $\bar{\alpha}$. It will be shown that the decoding process at the receiver is accomplished by the determination of the transmitted waveform over the constraint length of the code. This corresponds to the determination of the path through the trellis, taking into account the h_i in use in each symbol-period.

From finite state theory, the state matrix $L_{N,n}$ can be determined from the previous state:

$$L_{N,n} = L_{N,n-1} \cdot T_N = (T_N)^N$$

There are a number of interesting properties of this notation. $L_{N,n}$, the state location matrix, indicates whether or not a merging event has occurred when any element > 1. T_N, the state transition matrix can be defined in such a way as to delay as much as possible the first merge of the phase state. The number of signal states increases exponentially with the memory length $L-1$ of the state transition matrix. This "brute force" method has the advantage, however, of delaying the merge further without an increase in the number of phase states. Additional memory is required to maintain the arbitrarily chosen phase path during minimum distance calculations at the demodulator.

According to this method, the maximum constraint criteria can be expressed in a compact mathematical form. Let $C_{max} = 1 + K = 1 + log_2 N$, where $N = M^K$ is the number of signal states. Then in order for a maximum constraint code to exist, there exists a state transition matrix in the $(C_m - 1)$th symbol-interval, $T_N^{(C^m-1)}$, that must have no elements greater than one. This is in agreement with the original definition of T_N, since an element greater than one indicates a merge.

As a comparison to MSK, it is useful to use the example given for $N = 4$ as this is also the number of states for MSK $\left(0, \frac{\pi}{2}, \pi, \frac{3\pi}{2}\right)$. The state transition matrix, T_4 is chosen such that:

$$T_4 \cdot T_4 = \begin{bmatrix} 1 & 1 & 1 & 1 \\ 1 & 1 & 1 & 1 \\ 1 & 1 & 1 & 1 \\ 1 & 1 & 1 & 1 \end{bmatrix}$$

This is done to ensure the maximum constraint criteria given. By inspection of this matrix, there is more than one matrix which satisfies this criteria. The following is one example:

$$T_4 = \begin{bmatrix} 1 & 1 & 0 & 0 \\ 1 & 0 & 1 & 0 \\ 0 & 1 & 0 & 1 \\ 0 & 1 & 0 & 1 \end{bmatrix}$$

For any N, this form of the transition matrix can be expressed in general:

$$T_N = \begin{bmatrix} 1 & 0 & \cdot & \cdot & \cdot & 0 & 0 & 1 & 0 & \cdot & \cdot & \cdot & 0 & 0 \\ 1 & 0 & \cdot & \cdot & \cdot & 0 & 0 & 1 & 0 & \cdot & \cdot & \cdot & 0 & 0 \\ 0 & 1 & \cdot & \cdot & \cdot & 0 & 0 & 0 & 1 & \cdot & \cdot & \cdot & 0 & 0 \\ 0 & 1 & \cdot & \cdot & \cdot & 0 & 0 & 0 & 1 & \cdot & \cdot & \cdot & 0 & 0 \\ \cdots & \cdots & \cdots & \cdots & \cdots & \cdots & \cdots & \cdots & \cdots & \cdots & \cdots & \cdots & \cdots & \cdots \\ \cdots & \cdots & \cdots & \cdots & \cdots & \cdots & \cdots & \cdots & \cdots & \cdots & \cdots & \cdots & \cdots & \cdots \\ 0 & 0 & \cdot & \cdot & \cdot & 1 & 0 & 0 & 0 & \cdot & \cdot & \cdot & 1 & 0 \\ 0 & 0 & \cdot & \cdot & \cdot & 1 & 0 & 0 & 0 & \cdot & \cdot & \cdot & 1 & 0 \\ 0 & 0 & \cdot & \cdot & \cdot & 0 & 1 & 0 & 0 & \cdot & \cdot & \cdot & 0 & 1 \\ 0 & 0 & \cdot & \cdot & \cdot & 0 & 1 & 0 & 0 & \cdot & \cdot & \cdot & 0 & 1 \end{bmatrix}$$

The state transition equation $T_N^{(C_{max}-1)}$ is of the form:

$$T_N = \begin{bmatrix} \text{all 1} \\ N \times N \text{ Matrix} \end{bmatrix}$$

These general expressions may be re-arranged according to any form of equation 3.6 desired which results in the $T_4 \cdot T_4$ all 1 matrix. Other arrangements of these equations will not result in a simplified structure, however, since the constraint length and number of signal states remain the same. Fonseka indicates this T_4 has a constraint length of $C = 3$ and $d^2_{min} = 3$, which is exactly that of the multi-h set $H_K = \{\frac{1}{4}, \frac{2}{4}\}$.

3.7 Multi-T Coded CPFSK

Holubowicz and Szulakiewicz have presented a *Multi-T* form of this coding by assuming a set of non-uniform discrete symbol-intervals [10]. In this case, an average symbol-interval is defined:

$$T_{avg} = \frac{T_1 + T_2 + T_3 \ldots T_K}{K},$$

and, the modulation index in the nth interval is:

$$h_n = \Delta f \cdot T_n$$

Here, T is defined as follows:

$$(T_1, T_2, \ldots, T_K) = (\lambda_1 T, \lambda_2 T, \ldots, \lambda_k T)$$

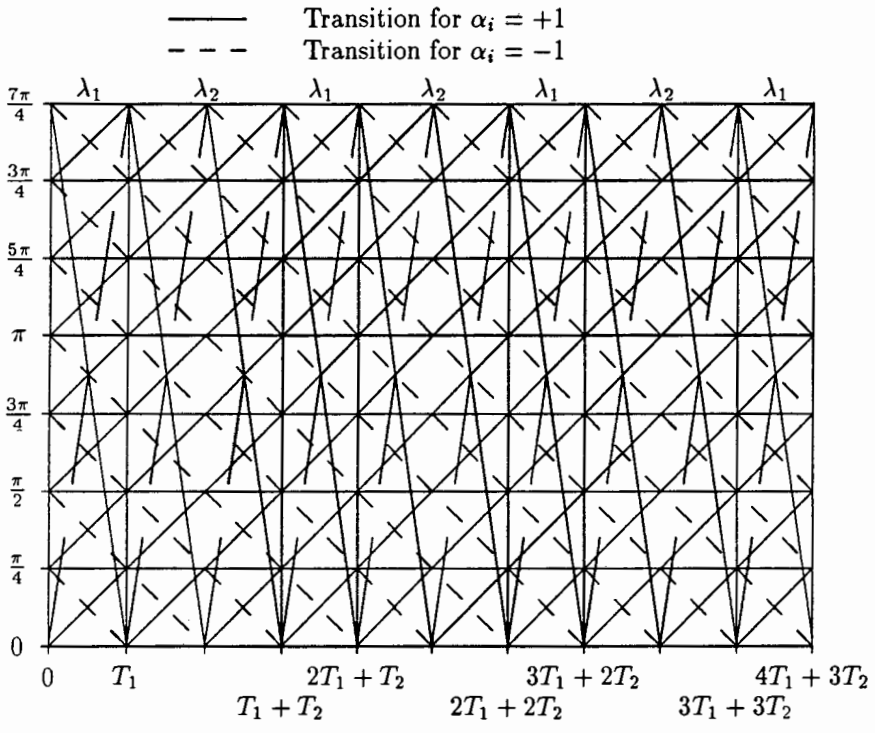

Figure 7: A phase trellis for Multi-T phase coding.

and

$$\lambda_i = \frac{h_i}{h_{avg}}$$

where:

$$h_{avg} = \frac{h_1 + h_2 + \ldots + h_K}{K}$$

A $H_K = \left\{\frac{1}{4}, \frac{2}{4}\right\}$ code becomes $(\lambda_1, \lambda_2) = (\frac{2}{3}, \frac{4}{3})$, with $h_{avg} = \frac{3}{8}$.

There is an interesting and subtle difference in this form of coding. Using the same form of phase trellis used previously, the multi-T phase trellis is shown in figure 7. Note that there are only ±one slopes here as compared to ±two slopes for the binary 2-H case. This means there are only two frequencies generated at the modulator as compared to four for $H_K = \left\{\frac{1}{4}, \frac{2}{4}\right\}$.

The Euclidean distance, d^2, of this code is:

$$\begin{aligned} d^2(s_1(t,\bar{\alpha}), s_2(t,\bar{\alpha})) &= \sum_{n=1}^{L} d_n^2(s_1(t,\bar{\alpha}), s_2(t,\bar{\alpha})) \\ &= \int_{\sum_j^{n-1} T_j}^{\sum_j^n T_j} (s_1(t,\bar{\alpha}) - s_2(t,\bar{\alpha}))^2 dt \end{aligned}$$

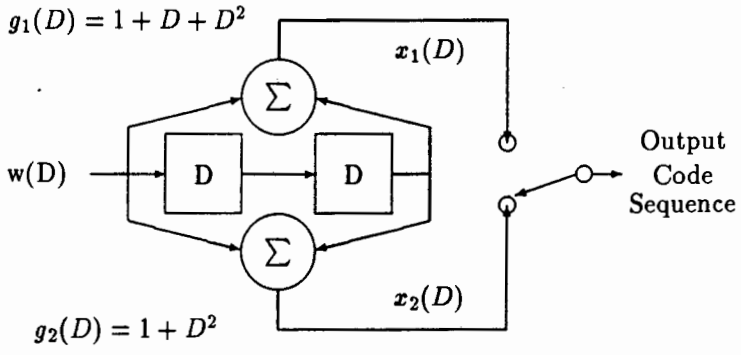

Figure 8: Rate $\frac{1}{2}$ convolutional encoder.

$$= \begin{cases} 2\lambda_n \left(1 - \frac{sin\Delta\phi_{n+1} - sin\Delta\phi_n}{\Delta\phi_{n+1} - \Delta\phi_n}\right), & \text{when } \Delta\phi_{n+1} \neq \Delta\phi_n \\ 2\lambda_n(1 - cos\Delta\phi_n), & \text{when } \Delta\phi_{n+1} = \Delta\phi_n \end{cases}$$

There is a trade-off for this scheme, however. Due to the non-uniform symbol- periods, the symbol rate would also be effected:

$$R_{avg} = \frac{\frac{1}{T_1} + \frac{1}{T_2} + \ldots + \frac{1}{T_K}}{K}$$

It is suggested, therefore, that in practice there will be no reduction in transmission bandwidth for comparable symbol rates. As the authors suggest, simplifications are possible by the reduction of the frequencies required at the modulator. This benefit, however, may be altered by the need for complexity to accommodate non-uniform bit-periods.

An interesting variant of multi-h coding occurs with the simultaneous use of data coding such as convolutional coding. This method of data coding is considered familiar to the reader. If the data vector $\bar{\alpha}$ is coded by the following shift register circuit as seen in figure 8, it can be seen by equation 1 on page 8 that the modulation index h_i and the data vector $\bar{\alpha}$ are independent. This will result in an increase in the number of phase states from qKM to qKM(K+L-2):

$$(\theta_n, \bar{D}_n) = (\theta_n, \bar{d}_{n-1}, \bar{d}_{n-2}, \ldots, \bar{d}_{n-K-L+2})$$

where L is the constraint length of the convolutional code [11]. The signal state vector is

$$X_n = (\bar{S}_n, \theta_n)$$

with $\bar{S}_n$ being a $\nu + l(L-1)$-tuple of information bits. It can be observed for any of the multi-h coded trellis so far that only q phase states exist in any one symbol period regardless of the set H_K. In general, there are $q \cdot 2^{\nu + l(L-1)}$ phase states. The separate coding effects of convolutional and multi-h coding may essentially be superimposed since both codes are considered linear.

As an example, consider the set $H_2 = \{\frac{1}{4}, \frac{2}{4}\}$, a r=$\frac{1}{2}$ convolutional coder, and a 4-ary CPFSK signal. As will be shown in later, there are 64 signal states associated with this particular set H_2 coded with four signal levels. Since a rate $\frac{1}{2}$ has a constraint length of 3, there are 64 multi-h states for each convolutional state from $X_n = (\bar{S}_n, \theta_n) = (0, 0, \frac{+3p\pi}{q}), (0, 0, \frac{+1p\pi}{q}), \ldots, (0, 0, \frac{-3p\pi}{q}),$. This results in a significant increase in the number of signal states for which receiver capacity must be increased. It is suggested, however, that the increase in receiver complexity for both methods could be minimal once the signal memory of *one* of these two methods were accomodated for.

4 Performance Criteria

4.1 Power Spectra

Consideration is now given to the spectral properties of Multi-h coding. There are four general methods of such calculations presented here, with the last being preferred due to it's accuracy. It is the intention of this treatment to identify the most accurate method of PSD calculation as a function of the set H_K in order to provide simplest comparison between various sets. The mathematical criteria for avoiding line spectra will also be shown here.

4.1.1 Method A: Simulation

A simulation approach is the simplest. A pseudo-random data sequence is digitally generated and is used to generate the modulation process. A discrete Fourier-transform, FFT for example, is used to directly compute the spectral content of the signal using the complex envelope form $e^{\phi(t_k)}$ for N samples. Using the expression $S(f) = |X_N(f)|^2$, where $X_N(f) = \sum e^{i\phi(t_k)} e^{-i2\phi f t_k}$, the PSD follows directly.

All of the classic characteristics of the FFT are applicable to computing the PSD in this way. This method approaches the exact signal spectrum only if the data sequence is quite long and perfectly random. Aliasing is an important concern with this method. The transient spectra introduced by a digitally sampled representation of a continuous-time signal will approach zero asymptotically as $\omega \rightarrow \infty$. Since the Fourier transform of a sampled sequence is a superposition of an infinite number of shifted Fourier transforms of the unsampled sequence scaled by $\frac{1}{T}$, it is important that aliasing considerations be made and thus avoided. If spectral estimates are desired at several times the symbol rate, a sampling rate of about sixteen times per symbol as suggested [15].

In addition to FFT characteristics of the computation, consideration must be given to the nature of the pseudo-random sequence. Only in the limit as $t \rightarrow \infty$ is each binary state in a data stream equiprobable. Since this is not practical in application, it is necessary to generate a sufficiently long pseudo-random sequence. To achieve accuracy comparable to a more exact method, an extremely high number of calculations is required. As an example, figure 9 is the result of a 4096 point FFT of 100,000 symbols.

4.1.2 Method B: Markov Processes

It has been shown that coded signals may be modelled as a Markov process [12]. This subject, as it applies to Multi-h coding, will be dealt with in detail in a later chapter. In consideration of spectral calculations, let the discrete state-space be the set of distinct modulator waveforms of modulo-2π phase at the symbol-boundaries. The signal is described as a sequence, or *Markov chain*, of all

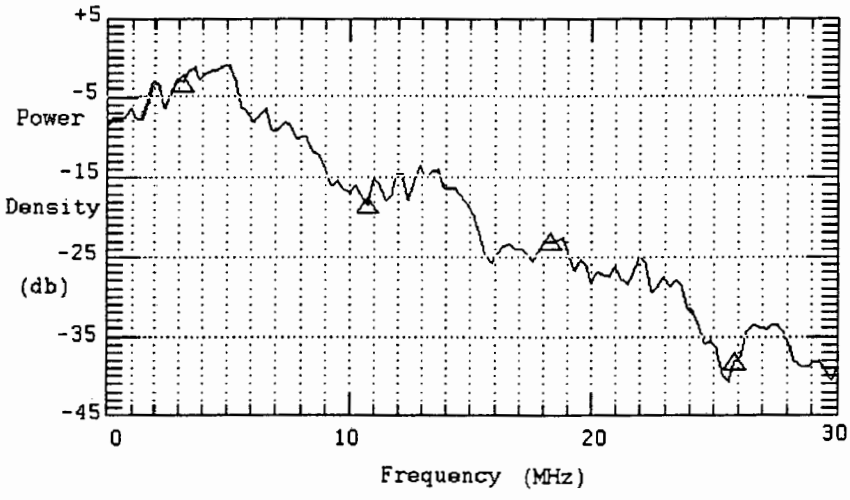

Figure 9: Power Spectral Density of $H_2 = \{\frac{1}{4}, \frac{2}{4}\}$ by simulation.

possible signals evolving among qKM states. Methods have been established to determine the spectra of signals which can be expressed in this way [13].

This method assumes the probabilities of any signal state being transmitted in two different symbol-periods, where the probability in symbol-period i is p_1 symbol-period j is p_2, and p_{12} is the transitional probability. The use of i and j denote two separate symbol periods, where $i \neq j$ Also, i=j+n, where $n > 1$. All possible signal states and transitions are equiprobable over the super-interval $T' = KT$. It is dependent, in part, on a particular path through the trellis (i.e. the on data vector $\bar{\alpha}$). A matrix, P, is formed describing the transitional probabilities between all possible paths. Noting that signal $s_1(t_1)$ lies in symbol-period i and $s_2(t_2)$ lies in symbol-period j, the auto-correlation function of these signals is:

$$r_{ij}(t_1;\tau_s) = \begin{cases} \sum_{t=1}^{qKM} p_1 \cdot p_{12}(j-1) \cdot s_1^*(t_1 - iT) \cdot s_2(t_2 - jT) & \text{if i}\neq\text{ j} \\ \sum_{t=1}^{qKM} p_1 \cdot s_1^*(t_1 - iT) \cdot s_1(t_2 - iT) & \text{if i=j} \end{cases}$$

The resultant expression for the power spectrum is derived from the Fourier transform of the auto-correlation functions just described [14]:

$$G(f) = \frac{1}{T} \sum_{j=1}^{N} \sum_{k=1}^{N} \sum_{n=-\infty}^{\infty} \frac{1}{N} e^{(i2\phi f nT)} P_{jk}^n S_j^*(f) S_k(f)$$

where N=qKM, and P_{jk}^n denotes the jk element of the state transition matrix P, raised to the nth power. Wilson suggests the major drawback of this scheme is the need to pay careful attention to state modeling of the multi-h code [15].

4.1.3 Method C: Auto-Correlation/Direct

There are several laborious approaches to the auto-correlation method [16]. In general, a classic auto-correlation function that results directly from the mathematical description of the time-continuous signal itself is found and a Fourier transform is performed for the PSD. In general, finding the *exact* auto-correlation is difficult if not impossible to find. This is the major constraint of this method. Assuming a properly derived function, this approach is generally accepted as the most accurate.

As a useful example [14], a low pass auto-correlation function is found over the ensemble of signals in the set at a fixed time, t_1 and is expressed in terms of the complex envelope:

$$\begin{aligned} R(t_1;\tau) &= E\left\{e^{[\phi(t_1+\tau)-\phi(t_1)]}\right\} \\ &= E\left[e^{j\Delta\phi}\right] \end{aligned}$$

Let $t_2 = t_2 + \tau$, where $nT \leq \tau(n+1)T$, $\tau = nT + \tau_s$. For multi-h coding, h_i and h_{i+n} are not equal unless n is an integer multiple of K. Let t_1 occur in symbol-period u and t_2 in symbol-period v. The phase difference between the two symbol-periods is:

$$\Delta\phi = a_u\omega_u[(u+1)T - t_1] + a_{u+1}\omega_{u+1}T + \cdots + a_{v-1}\omega_{v-1}T + a_v\omega_v(t_2 - jT)$$

This results in the following auto-correlation function:

$$\begin{aligned} R(t_1;\tau) &= E\left[e^{ia_u\omega_u[(u+1)T-t_1]}\right] \cdot E\left[e^{ia_{u+1}\omega_{u+1}T}\right] \cdots E\left[e^{ja_{v-1}\omega_{v-1}T}\right] \cdot E\left[e^{ja_v\omega_v[t_2-vT]}\right] \\ &= \sum_{v=0}^{\infty} r_{uv}(t_1;\tau_s), \qquad u \geq 0 \end{aligned}$$

where:

$$r_{vu}(t_1;\tau_s) = \begin{cases} cos(\omega_u\tau), & \text{u=v} \\ \prod_{k=u+1}^{v-1} cos(\omega_k T) \cdot E\left[e^{ia_u\omega_u[u+1]T-t_1]}\right] \cdot E\left[e^{ia_v\omega_v(t_2-vT)}\right], & \text{u} \neq \text{v} \end{cases}$$

If the domain of t_1 and t_2 is extended from a symbol-period to T'=KT where K is the number of indices in the set H_K, then this auto-correlation function is periodic with period K:

$$r_{u,v+K}(t_1;\tau_s) \;=\; \prod_{i=0}^{K-1} cos(\omega_i T \cdot r_{uv}(t_1;\tau_s)) \quad u \neq v$$

An important function is derived from this expression, that of the characteristic function:

$$C(1;T') = \prod_{i=0}^{K-1} cos(\omega_i T_s)$$

In order to have a line-free spectrum, it is necessary that:

$$|C(1;T_K)| < 1$$

This condition will be of use shortly.

In the case of multi-h CPFSK, expressions which approximate spectra have been given. The mean of H_K may be taken, with the result applied to an expression for constant-h CPFSK:

$$G(f) = G_+(f) + G_-(f)$$

where:

$$G_\pm(f) = \frac{A^2 sin^2[\pi(f \pm f_1)T_s] sin^2[\pi(f \pm f_2)T_s]}{2\pi^2 T_s\{1 - 2cos[2\pi(f \pm \alpha)T_s]cos(2\pi\beta T_s) + cos^2(2\pi\beta T_s)\}} \times \left[\frac{1}{f \pm f_1} - \frac{1}{f \pm f_2}\right]^2$$

T_s = Symbol Duration

A = Signal Amplitude

f_1, f_2 = Signal frequencies in Hz

$= f_c \pm \frac{h}{2T_s}$ Hz, where f_c is the center frequency

$\alpha = \frac{1}{2}(f_2 + f_1)$

$\beta = \frac{1}{2}(f_2 - f_1)$

These equations are used to compute the following approximation for the spectra:

$$G(f) \simeq \frac{1}{K} \sum_{i=1}^{K} G_{h_i}(f) \tag{7}$$

A more exact approach has been suggested whereby the Fourier transform of the deterministic signal is performed, and then ensemble averaged over the $\bar{\alpha}$ and ϕ:

$$\lim_{N\to\infty} \frac{1}{NT_s} E\left\{|S_N(f,\bar{\alpha})|^2\right\}$$

The numerical Fourier-transformation is used and numeric integration is required [15]. As will be seen, this method does not necessarily utilize FFT methods. Numeric integration is used to compute the transform. Here, the spectra derived is a direct function of the indices and number of signal levels

used. Mazo and Salz give generalized closed form expressions for generalized Frequency Modulated signals, and then develop the expressions for random waveforms [17]. From this, Wilson derived a natural extension for multi-h. In the most general sense of finding the deterministic expression, this method can be as tedious as any of the auto-correlation methods. The advantage here, however, is in the application to multi-h coded signals- a single closed-form solution is possible for *any* set H_K. The entire derivation is not reproduced here, however, the expression and a brief description is stated as the result is an important one.

The closed form expression by Mazo is for arbitrary, random, frequency modulated waveforms. Wilson then uses this result to define multi-h as a distribution of a set of possible waveforms which exist for the set H_K over the interval $T' = KT_s$. T' is referred to as a super-baud in some literature [1]. If all signals in the distribution over T' are considered stochastic and equiprobable, the result is exact over the set of signals considered. Citing a definition of Rice [18] for power spectrum:

$$G(f) = \lim_{\lambda \to \infty} \frac{2}{\lambda} G_\lambda(f),$$

where

$$G_\lambda(f) = E\left\{ \left| \int_0^\lambda X(t) e^{-i2\pi f t} dt \right|^2 \right\},$$

Mazo and Salz [17] combine the auto-correlation function and Fourier-transform expression for any two signals in the set under consideration as follows:

$$G_\lambda(f) = E\{ \sum_{k=0}^{N-1} \sum_{s=0}^{N-1} \int_{kT}^{(k+1)T} \int_{sT}^{(s+1)T} X(t_1) X^*(t_2) \cdot e^{i2\pi f(t_2 - t_1)} \}$$

where $\{s_n(t), n = 0, 1, ...\}$ is a sequence of independent, stochastic signals defined in an interval [0,T], and:

$$X(t) = e^{i \int_0^t \Psi(\tau) d\tau}$$

where

$$\Psi(t) = \sum_{n=0}^{\infty} s_n(t - nT)$$

This expression is manipulated giving $G_\lambda(f)$ as a function of the signals in the set under consid-

eration, with the result:

$$G(f) = \frac{2}{T'}[P(f) + 2Re\{F(f)F_b^*(f)e^{-i2\pi fT'} + F(f)F_b^*(f)\Gamma(f)\}]$$

where:

$$\Gamma(f) = e^{-i4\pi fT'}\frac{C(T')}{1 - C(T')e^{-i2\pi fT'}}$$

$$b_n(t) = \int_0^t s_n(\tau)d\tau, \quad b_n \equiv b_n(T) \tag{8a}$$

$$B_n = b_n(T') \tag{8b}$$

$$F_n(f) = \int_0^{T'} e^{-i2\pi ft + ib_n(t)}dt \tag{8c}$$

$$C(T') = E\{e^{iB_n} = M^{-K}\sum_n F_n(f)\} \tag{8d}$$

$$F(f) = E\{F_n(f)\} = M^{-K}\sum_n F_n(f) \tag{8e}$$

$$F_b^*(f) = E\{F_n^*(f)e^{iB_n}\} = M^{-K}\sum_n F_n^*(f)e^{iB_n} \tag{8f}$$

$$P(f) = E\{|F_n(f)|^2\} \tag{8g}$$

$$= M^{-K}\sum_n |F_n(f)|^2. \tag{8h}$$

$$\tag{8i}$$

For the multi-h case, $b_n(t)$ is:

$$\begin{aligned} b_n(t) &= \pi\int_0^t [d_{1n}h_1 g(\tau) + d_{2n}h_2 g(\tau) + \cdots + d_{Kn}h_K g(\tau - KT)]d\tau, \\ &\triangleq \pi\int_0^t f_n(\tau)d\tau, \\ &\quad \text{n=1,2,...,}M^K \end{aligned} \tag{9}$$

This compact form is only a function of the symbol-period, the modulation index set H_K, data set ($\{\pm 1, \pm 2, ..., \pm(M-1)\}$), and the pulse shape g(t). Upon initial examination of these results, one may wonder why this expression has been so defined. Each function is a useful description of key characteristics of the signal set. By examination of the initial expression for equation 1, it can be seen that $b_n(t)$ is an expression for accumulated phase. For this set of equations it is convenient to define a characteristic function B_n, the random phase accumulation over T'=KT seconds. Further the characteristic function C(T') is the same one derived from the work of Lereim. B_n terms lie on a

linear lattice. If no premature merger has occurred, each term may be described as a distinct point on a line and symmetrical to the origin.

$$\begin{aligned} B_1 &= 2\pi j_1 \\ B_2 &= 2\pi j_2 \\ &\vdots \quad \vdots \\ B_{M^K} &= -2\pi j_1. \end{aligned} \tag{10}$$

In matrix form, [A][h]=2[j], where [A] is defined as a $M^K \times K$ matrix and whose rows consist of all possible K-tuples with elements selected from the M-ary set $\{\pm 1, \pm 3, \cdots, -(M-1)\}$. A generalized expression of this matrix is not practical here in consideration of space since the matrix dimensions increase very rapidly with M and K. As an example with K=3 ($H_K = \{h_1, h_2, h_3\}$) and M=2 ($\bar{\alpha} \in \{\pm 1, \pm 3\}$), the result is a 8×3 array:

$$\bar{A} = \begin{bmatrix} +1 & +1 & +1 \\ +1 & +1 & -1 \\ +1 & -1 & +1 \\ +1 & -1 & -1 \\ -1 & +1 & +1 \\ -1 & +1 & -1 \\ -1 & -1 & +1 \\ -1 & -1 & -1 \end{bmatrix}$$

Solutions for equation 10 and for C(T')=1 occur for integer values of h_i. The number integer indices which create line spectra are dependent upon M and K. Let:

$$\bar{D} = \bar{A}^T,$$

then the data vectors, $\bar{d}$, of equation 10 are a partitioned sub-set of$\bar{D}$.

The benefit of a closed-form solution for the PSD is to readily provide techniques for the comparison between different H_K. Since transmission bandwidth is also a function of h, spectral considerations are also to be made. Spectral lines exist for integer indices and are to be avoided. Spectrally conservative indices are typically < 1. An aim of this treatment on the subject is to investigate forms of multi-h which are practical in implementation.

The phase-difference state defined for a pair of sequences is determined by the mod-2π phase difference. The minimum Euclidean distance exists between $t = 0$ and the first merge, or bisection, of

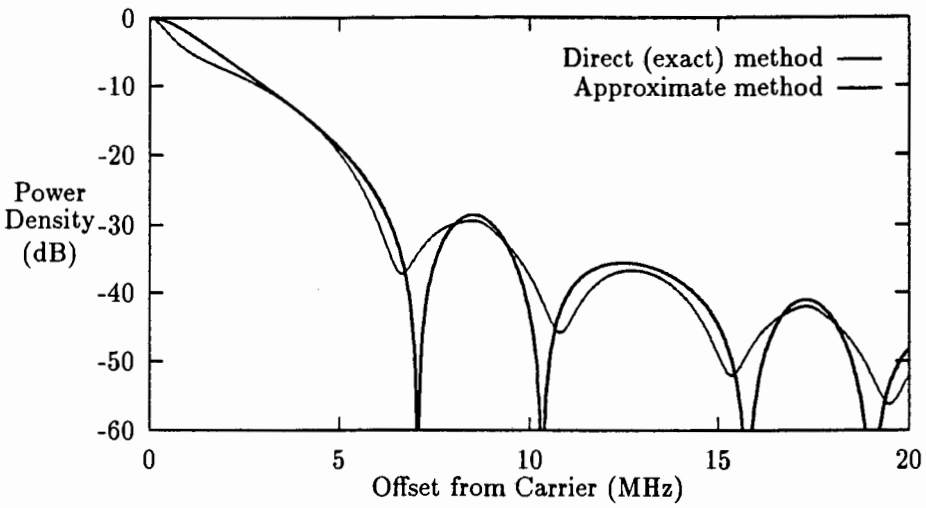

Figure 10: Comparison of direct methods of PSD calculations for Multi-h coded CPFSK signals.

the paths of any two possible progressions through the trellis. The bit-error improvement is realized by delay in this merge which corresponds to an increase over the pre-merge phase difference expression.

PSD calculation by approximate and exact methods are shown in Figure 10. The approximate is considered poor due to it's representation of minima as nulls, when no such nulls actually exist in the spectrum. The absence of nulls is a result of the coding method. Intuitively, it can be predicted by consideration of the PSD of each h_i. Each will have it's own precise null which disappears over the ensemble average over T' by the other PSD in the set H_K.

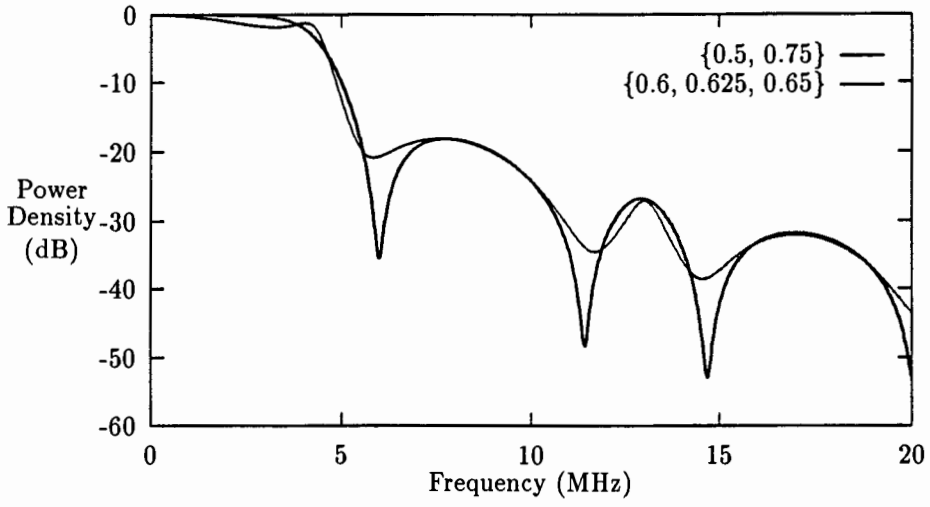

Figure 11: The exact PSD of two multi-h coded CPFSK signals with H_K of same mean but different variance.

Figure 11 shows the effect the standard variation has on the spectra. Both spectra have the same mean of 0.625. This 3-H set, however, has a smaller statistical variance. This has the effect of a greater degree of partial overlap of the nulls for each element in the H_K set. This results in deeper minima.

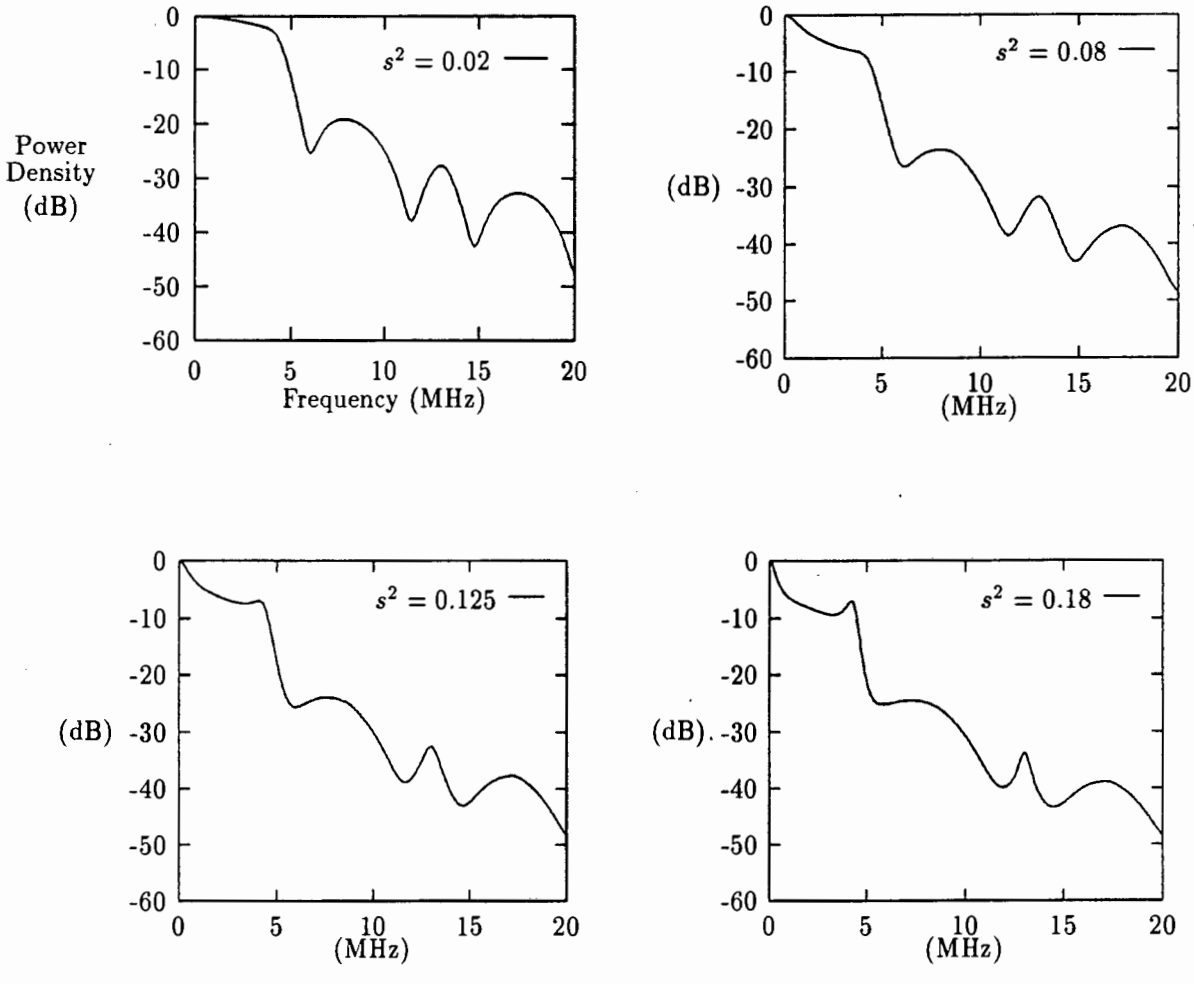

Figure 12: Comparison of the spectral properties for different statistical variance of H_K sets.

The main lobe behavior is also predicted by the statistical variance, as shown in figure12. It can be seen that for greater s^2, attenuation of the main lobe happens at a higher frequency and drop-off is more rapid. The minima, however, remains the same. Sidelobe attenuation remains relatively the same. Additional minima occur for higher s^2.

4.2 Error Performance

To realize the decrease in error probability offered by multi-h coding, it is beneficial to examine the treatment of the error probability of Fast Frequency Shift Keying done by DeBuda [5]. This paper discusses the notion of using the signal phase, as well as the signal frequency, to achieve a decrease in the error probability during the demodulation process. This results in significant improvement of receiver performance. In order to decode the information sent during a particular symbol-period, a delay is made due to the decision at the receiver in observing the signal phase for a sufficient period of time so as to determine the phase state of the signal. This introduction of memory into the receiver does result in an increase in complexity, but the gain in error performance is sufficient justification. This technique is also used for PSK and ASK.

As an example, a continuous-phase binary FSK signal is chosen with a constant modulation index of $h = \frac{1}{2}$. While any modulation index can be used, for binary line codes this modulation index results in a minimum number of symmetric phase states, $(0, \frac{\pi}{2}, \pi, \frac{3\pi}{2})$. The result is the starting phase at the symbol-boundary of every other symbol-period will either be 0 or π. In the remaining symbol-periods, it will be either $\frac{\pi}{2}$ or $\frac{3\pi}{2}$. Mathematically, the need to observe the the signal over an additional symbol-period for information recovery is realized by comparison of the following mathematical expression for the signal over one and two symbol-periods:

$$u(t) = \begin{cases} +e^{i\left(\omega t \pm \frac{\pi t}{2T}\right)}, & \\ & \phi(0) = \begin{cases} 0, \\ \pi, \end{cases} \\ -e^{i\left(\omega t \pm \frac{\pi t}{2T}\right)}, & \\ & 0 \le t \le T. \end{cases}$$

Over a second symbol-period:

$$u(t) = \begin{cases} \mp e^{i\left(\omega t \pm \frac{\pi t}{2T}\right)}, & \\ & \phi(-T) = \begin{cases} \frac{\pi}{2}, \\ \frac{3\pi}{2}, \end{cases} \\ \pm - e^{i\left(\omega t \pm \frac{\pi t}{2T}\right)}, & \\ & -T \le t \le 0. \end{cases}$$

The sign of each term in the second interval depends on the sign of the first and second symbol-interval. These two expressions may be combined using the relation:

$$Re\left\{e^{i\left(\pm \frac{\pi t}{2T_s}\right)}\right\} = cos\left(\frac{\pi t}{2T_s}\right)$$

Combining the expression for the two symbol-periods:

$$Re\{u(t)e^{-i\omega t}\} = \begin{cases} +cos\left(\frac{\pi t}{2T_s}\right), & \phi(0) = \begin{cases} 0, \\ \pi, \end{cases} \\ -cos\left(\frac{\pi t}{2T_s}\right), & \\ & -T \leq t \leq T. \end{cases}$$

For the alternate symbol-periods, where the phase states are $\{\frac{\pi}{2}, \frac{3\pi}{2}\}$, the complex signal expressions in each interval:

$$u(t) = \begin{cases} +e^{i\left(\omega t \pm \frac{\pi t}{2T}\right)}, & \phi(T) = \begin{cases} \frac{\pi}{2}, \\ \frac{3\pi}{2}, \end{cases} \\ -e^{i\left(\omega t \pm \frac{\pi t}{2T}\right)}, & \\ & T \leq t \leq 2T, \end{cases}$$

$$u(t) = \begin{cases} \mp e^{i\left(\omega t \pm \frac{\pi t}{2T}\right)}, & \phi(0) = \begin{cases} 0, \\ \pi, \end{cases} \\ \pm - e^{i\left(\omega t \pm \frac{\pi t}{2T}\right)}, & \\ & 0 \leq t \leq T, \end{cases}$$

combine to form:

$$Re\{u(t)e^{-i\omega t}\} = \begin{cases} +sin(\frac{\pi t}{2T_s}), & \phi(T) = \begin{cases} \frac{\pi}{2}, \\ \frac{3\pi}{2}, \end{cases} \\ -sin(\frac{\pi t}{2T_s}), & \\ & 0 \leq t \leq 2T. \end{cases}$$

All that is necessary, then, is to observe the signal over two symbol-intervals in both frequency *and* phase coherence and determine whether one of two antipodal sinusoidal signals have been sent. Because this is the same determination as that made in a coherent binary (antipodal baseband) receiver, the same probability of error applies [1]:

$$P_e = \frac{1}{2\pi} exp\left(-\frac{E_b}{N_o}\right)$$

This is 3 dB gain over non-coherent FSK [5]:

$$P_e = \frac{1}{2} exp\left(-\frac{E_b}{2N_o}\right)$$

The probability of error for multi-h CPFSK codes is [7]:

$$P_e = Q\left[d(1,2)\sqrt{\frac{E_b}{2N_o}}\right]$$

For a given $\frac{E_b}{N_o}$, it can be seen that the probability of error is dependent on the distance properties of the code. Anderson and Taylor show this by using a alternative form for the CPFSK signal to derive an error expression for multi-h codes:

$$s(t) = \sqrt{\frac{2E_s}{T_s}} cos\left(\omega_c t + \Omega_i t + \theta_i\right)$$

Since coherence is assumed, θ_i is constant over the symbol-period. $\Omega_i = \frac{2\pi h_i}{T_s}$ is a frequency deviation over the interval. The d^2 distance for a symbol-interval is:

$$\begin{aligned}\int_{nT_s}^{(n+1)T_s} (s_1 - s_2)^2 dt &= \int s_1^2 dt + \int s_2^2 dt - 2\int s_1 s_2 dt \\ &\approx 2E_b - 2\int s_1 s_2 dt, \qquad \text{for } \omega_c \text{ large.}\end{aligned}$$

Substituting the expression for s(t) above:

$$\frac{2E_b}{T_s}\int cos(\omega_c t + \Omega_1 t + \theta_1) cos(\omega_c t + \Omega_2 t + \theta_2) dt = \frac{E_b}{T_s}\frac{sin[(\Omega_1 - \Omega_2)t + (\theta_1 - \theta_2)]}{\Omega_1 - \Omega_2}\Bigg|_{t=nT_s}^{(n+1)T_s} + \epsilon,$$

where $\epsilon \rightarrow 0$ as $\omega_c \rightarrow \infty$. If:

$$\begin{aligned}\Delta_{n+1} &= (\Omega_1 - \Omega_2)(n+1)T + (\theta_1 - \theta_2) \\ \Delta_n &= (\Omega_1 - \Omega_2)nT + (\theta_1 - \theta_2)\end{aligned}$$

is the total phase differences at the end and beginning of each interval. The result is, assuming $\omega_c \gg \frac{2\pi}{T_s}$:

$$d^2 = \begin{cases} 2\left(1 - \frac{sin\Delta\phi_{n+1} - sin\Delta\phi_n}{\Delta\phi_{n+1} - \Delta\phi_n}\right) & \Delta\phi_{n+1} \neq \Delta\phi_n \\ 2(1 - cos\Delta\phi_n) & \Delta\phi_{n+1} = \Delta\phi_n \end{cases}$$

where $\Delta\phi_n$ and $\Delta\phi_{n+1}$ are the phase difference between the two signals, s_1 and s_2, in any two consecutive intervals. Note that the $\Delta\phi$ is an absolute difference and not modulo-2π. The d^2_{min} (as defined previously) of good codes does not vary excessively from interval to interval, unlike bad codes. That is, given the phase difference of each interval over a number of symbol periods concerned, the standard deviation of all $\Delta\phi$ is small for a good code.

As with the uncoded case, multi-h coded CPFSK is piecewise-continuous. The probability of error follows, then, the same error function as in the uncoded case subject to d^2_{min} improvements of the H_K set:

$$P_e \approx \left(\sqrt{\frac{d^2_{min} E_b}{N_o}}\right)$$

From the nature of Gaussian distribution, it follows that the improvement to P_e through the coding is highly dependent on the state of $\frac{E_b}{N_o}$. Note also that since this is normalized to the symbol-energy. Since $D^2 = 2E_b d^2$, it follows that higher signal densities are required to achieve the coding gain for higher levels of signaling.

Since the intention of coding is to decrease the amount of power needed to maintain a particular bit-error rate, of consideration of how much coding gain can be achieved with minimal impact to the spectral content and complexity in implementation of the method given. As will be shown, the increase in d^2_{min} corresponds to an increase in the distance between message points in signal space. This corresponds to a large temporal separation on the phase trellis.

Multi-h coding is different from data coding because the waveform itself is altered and not the information being carried. This subtle difference means that the decoding of multi-h signals is only done by the measurement of signals rather than the binary processing of the received information. The implemented structures use a soft form of detection rather than hard limiting, and are considered to be more robust in the presence of noise as a result. This determines the characteristics of the error performance to a large degree. As the size of the set H_K is increased, multi-h coded signals maintain their integrity for higher amounts of noise.

An observation made by Anderson is that for sufficiently large $\frac{E_b}{N_o}$, determination of the correct data at the receiver is determined largely by d^2_{min}. This is where multi-h coding is found to be most useful. The benefits of any method of coding appear to vanish rapidly for low $\frac{E_b}{N_o}$. This is also true of multi-h codes. By experimentation McLane [19] has shown by simulation that in the presence of

fading, multi-h coding maintains it's error probability. This is due to the multiple frequency-shift nature of the coded signal as compared to the fewer signal points of the uncoded signal. This is referred to as *frequency diversity* .

5 Transmitter Structures

5.1 A Markov Representation

Markov theory is usually applied to the theory of demodulation. Since the modulator produces a sequence of a finite set of waveforms, it is applicable to the modulator. It is presented here in the context of a set of multi-h coded waveforms.

Let a particular stochastic state at a specific point in time $t = iT$ occur with a probability, P_i. This probability, in general, is a function of the probabilities of all previous states which occurred:

$$P_1 = P\{X_1 = i_1 | X_0 = i_0\}$$
$$P_2 = P\{X_2 = i_2 | X_1 = i_1 | X_0 = i_0\}$$
$$P_3 = P\{X_3 = i_3 | X_2 = i_2 | X_1 = i_1 | X_0 = i_0\}$$

The class of stochastic processes of concern in this work are those whose probabilistic dependence on previous states are manifest only on the most immediate previous state. In other words, the stochastic state of the current process is determined only by the previous state. This type of process is referred to as a *Markov Process.* It is in this context that the progression of multi-h coded CPFSK waveforms will be discussed as a Markov chain. For such processes, if:

$$P\{X_1 = j | X_0 = i\} = P\{X_2 = j | X_1 = i\} = \ldots = P\{X_k = j | X_{k-1} = i\},$$

then the process is considered stationary for all symbol periods k=0,1,2,...,k [20]. This property permits significant mathematical simplifications as will be shown.

Let each phase state associated with a set H_K be described by an integer {1,2,...,qKM}, where qKM is the number of phase states of the multi-h code. As a stochastic process, it may be assumed that the conditional probability of a particular phase state at time $t = iT$ is a function of the conditional probabilities of each previous symbol-period. For example, for i=4:

$$\begin{aligned}
&P\{X_0 = \phi_0(t,\bar{\alpha}), X_1 = \phi_1(t,\bar{\alpha}), X_2 = \phi_2(t,\bar{\alpha}), \text{and} X_3 = \phi_3(t,\bar{\alpha}\} \\
&= P\{X_3 = \phi_3(t,\bar{\alpha}) | X_2 = \phi_2(t,\bar{\alpha}), X_1 = \phi_1(t,\bar{\alpha}), X_0 = \phi_0(t,\bar{\alpha})\} \\
&\times P\{X_2 = \phi_2(t,\bar{\alpha}) | X_1 = \phi_1(t,\bar{\alpha}), X_0 = \phi_0(t,\bar{\alpha})\} \\
&\times P\{X_1 = \phi_1(t,\bar{\alpha}) | X_0 = \phi_0(t,\bar{\alpha})\} \\
&\times P\{X_0 = \phi_0(t,\bar{\alpha})\}
\end{aligned}$$

Because this is a Markov process, the following conditional probabilities apply:

$$P\{X_3 = \phi_3(t,\bar{\alpha})|X_2 = \phi_2(t,\bar{\alpha}), X_1 = \phi_1(t,\bar{\alpha}), \text{and} X_0 = \phi_0(t,\bar{\alpha}\}$$
$$= P\{X_3 = \phi_3(t,\bar{\alpha})|X_2 = \phi_2(t,\bar{\alpha})\}$$
and
$$P\{X_2 = \phi_2(t,\bar{\alpha})|X_1 = \phi_1(t,\bar{\alpha}), X_0 = \phi_0(t,\bar{\alpha})\} = P\{X_2 = \phi_2(t,\bar{\alpha})|X_1 = \phi_1(t,\bar{\alpha})\}$$
this results in the following simplified expression:
$$P\{X_0 = \phi_0(t,\bar{\alpha}), X_1 = \phi_1(t,\bar{\alpha}), X_2 = \phi_2(t,\bar{\alpha}), \text{and} X_3 = \phi_3(t,\bar{\alpha})\}$$
$$= P\{X_3 = \phi_3(t,\bar{\alpha})|X_2 = \phi_2(t,\bar{\alpha})\}\, P\{X_2 = \phi_2(t,\bar{\alpha})|X_1 = \phi_1(t,\bar{\alpha})\}$$
$$\times P\{X_1 = \phi_1(t,\bar{\alpha})|X_0 = \phi_0(t,\bar{\alpha})\}\, P\{X_0 = \phi_0(t,\bar{\alpha})\}$$

The stationary nature permits the following simplification. Given two possible phase states $\phi_1(t,\bar{\alpha})$ at $t = T_s$ and $\phi_2(t,\bar{\alpha})$ at $t = 2T_s$, the transitional probabilities between the states are completely determined by:

$$P\{X_1 = \phi_1(t,\bar{\alpha})|X_0 = \phi_1(t,\bar{\alpha})\} = P\{X_k = \phi_1(t,\bar{\alpha})|X_{k-1} = \phi_1(t,\bar{\alpha})\},$$

$$P\{X_1 = \phi_2(t,\bar{\alpha})|X_0 = \phi_1(t,\bar{\alpha})\} = P\{X_k = \phi_2(t,\bar{\alpha})|X_{k-1} = \phi_1(t,\bar{\alpha})\},$$

$$P\{X_1 = \phi_1(t,\bar{\alpha})|X_0 = \phi_2(t,\bar{\alpha})\} = P\{X_k = \phi_1(t,\bar{\alpha})|X_{k-1} = \phi_2(t,\bar{\alpha})\},$$

$$P\{X_1 = \phi_2(t,\bar{\alpha})|X_0 = \phi_2(t,\bar{\alpha})\} = P\{X_k = \phi_2(t,\bar{\alpha})|X_{k-1} = \phi_2(t,\bar{\alpha})\}$$

This may be generalized to include any phase states at any symbol-interval of a multi-h coded CPFSK signal under consideration.

Two different Markov processes will be considered. One is for phase states. The other is for signal states. There is a one-to-one correspondence between these two types, but each will be used in a slightly different manner to describe the signals and the structure used to implement them.

5.2 Single Oscillator Implementation

One method of generating a CPFSK waveform is with a VCO, as shown in figure 13 for a 2-H scheme. It is assumed that there is sufficient damping in the oscillator feedback loop to ensure a continuous phase signal at the modulator output.

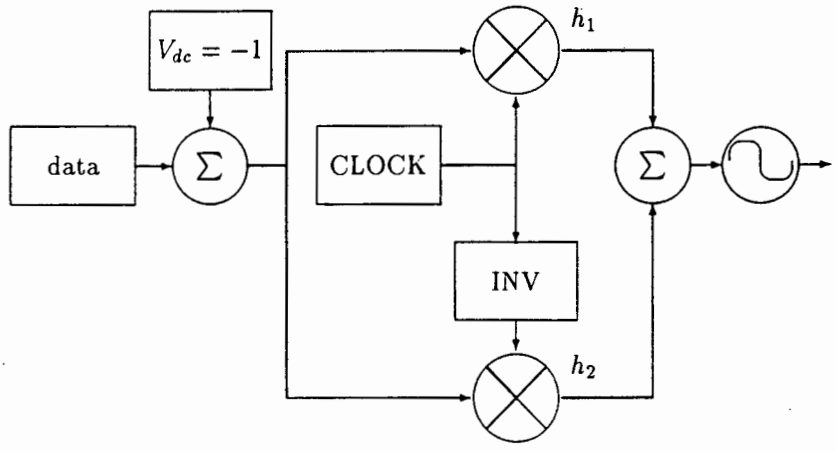

Figure 13: A simple 2-h VCO modulator.

5.3 Multiple-Oscillator Implementation

5.3.1 Massey Modulator Structure

As an alternative to the single VCO circuit, Massey has suggested a multiple oscillator form of structure [21]. For this purpose, the continuous-phase MSK waveform is expressed alternatively:

$$s(t) = x(i)p(t) + y(i)q(t)$$
$$iT_s \leq t < iT_s + T_s$$

where T_s is the symbol period and y(i), x(i) assume ternary values {+1, 0, -1}.

Consider the I-Q structure in figure 14(a).

If:

$$p(t) = A\sin\left[\left(\omega_o + \frac{\Delta\omega}{2}\right)t + \theta\right] \tag{11}$$
$$q(t) = A\sin\left[\left(\omega_o - \frac{\Delta\omega}{2}\right)t + \theta\right]$$

$$a(i) = 1, \text{ all i} \tag{12}$$
$$b(i) = (-1)^{i+1}$$

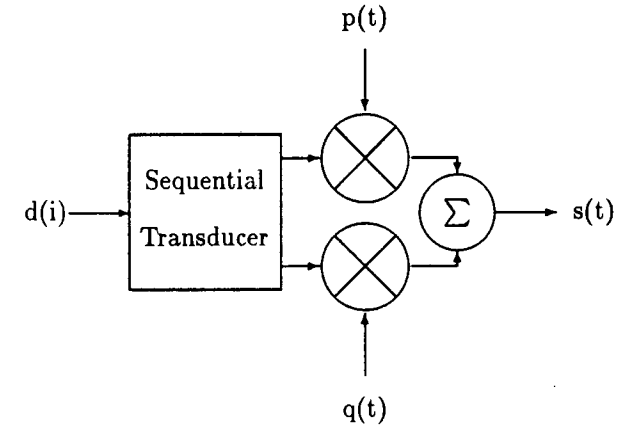

(a) Modulator Structure

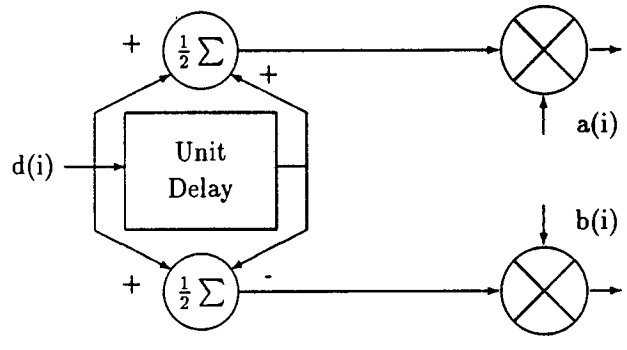

(b) Sequential Transducer

Figure 14: Massey MSK Structure.

5.3.2 Massey Transducer/Coder

It can be seen from figure 14(a) that an implementation of equation 12 provides bipolar switching between the two oscillators. The ternary outputs of the transducer provide a phase diversity of π radians for each oscillator shown in figure 14(b). Only one transducer output has a non-zero output in any given symbol-interval. Note that this structure does not only apply to MSK, but does so only if a(i) and b(i) are defined by equations 12 and 13. This ternary transducer is the key to a significant simplification of the multi-oscillator modulator while switching each oscillator to the output in such a way as to maintain a continuous phase signal for all i.

5.3.3 A Generalized Multi-Oscillator Structure

To describe an appropriate structure for a greater number of signaling frequencies, consider first again the case for the MSK structure. Each frequency and phase is a distinct state. Let $-\Delta f$ represent bipolar data -1 (or binary 0), and $+\Delta f$ a bipolar data +1 (or binary 1). Each signal frequency can assume one of two phase states:

$$\begin{array}{ll} (-\Delta f, 0) & (+\Delta f, 0) \\ (-\Delta f, \pi) & (+\Delta f, \pi) \end{array}$$

It is very important to understand that the phases given for each frequency are with respect to the actual signal frequency- not the center frequency f_o. It is these four signal states that the modulator must generate. This is a subtle but important difference to the conventional phase states usually expressed for MSK.

Each of these states and the transitions which exist between them is a function of the data vector, $\bar{\alpha}$, and shown in figure 16. Each signal state is shown in figure 15. An important observation of the MSK states is there are only two phase states for these four signal states (0,π). In other words, for each phase state there exists two signal states (one for each frequency shift). This a key to the simple oscillator and transducer network given by Massey. It is believed that use of this characteristic could be made in the design of a ternary form a generalized transducer implementing a greater number of signal frequencies.

5.4 Multi-Oscillator Implementation for the Set $H_2 = \left\{\frac{1}{4}, \frac{3}{4}\right\}$

A different form of phase trellis is now presented. Recall that the signal frequency $f = f_o \pm \frac{h_i}{2T_s}$ for a particular symbol period. In conventional form of trellis, the phase states at the symbol boundaries were with respect to f_o. They key to understanding this different form of trellis is that the current phase states are with respect to *the current signal frequency f.*

To illustrate this important difference, all waveforms for every possible signal state of MSK are

shown in figure 15. Assume the phase $\phi = 0$ at $t = 0$, and that a waveform corresponding to $+f = f_o + \frac{h}{2T_s}$ where h=$\frac{1}{2}$. If $-f = f_o - \frac{h}{2T_s}$ is transmitted for the second interval, a phase shift by π must be made to an frequency source a -f Hz to maintain continuity at the symbol boundary. No shift in phase would be necessary of +f were to be transmitted during the second interval. This result is shown on the multi-oscillator trellis for MSK in figure 16.

For the Multi-h coded CPFSK case of the set $H_2 = \{\frac{1}{4}, \frac{3}{4}\}$, waveforms representing all possible signal states are shown in figure 17 and 18. For the multi-oscillator shown in figure 19, $+h_2$ represents a data +1 in a symbol interval using a modulation index of h_2, this corresponds to the generation of a frequency shift of $+\frac{\pm h_2}{2T_s}$ Hz from the center frequency, ω_o. For the diagrams presented, $\pm h_i$ corresponds to $\pm f = f_o \pm \frac{h_i}{2T_s}$. $+h_2 \rightarrow \pm h_1$ denotes a transition between two states where the the previous data symbol was +1 using h_2, with the current data symbol is either ± 1 using a h_1 modulation index.

A binary coding circuit representation of this multi-oscillator trellis may be found by considering a starting phase of $\phi = 0$, and developing a logic circuit which mimics the Markov chain. This coder is similar to the original Massey structure as shown in figure 14(b), but with binary outputs. The trellis of figure 19 has a period of C+1 where the constraint length of the code is C=3. From this it can be seen by examination of this trellis that there are two separate signal states for each phase. If a simplification of this trellis is made just to illustrate the transition between the current and previous phases, figure 20 is the result. For each transition, the previous and current signaling frequency and the applicable modulation index is shown.

Note that only the most immediate previous state is needed is due to the Markov property of the process. It can also be seen how the previous state is inherently due to all previous states before it.

The resulting circuit shall have binary outputs with only one output in a high state in any symbol-interval. For a particular symbol interval, the coder output which is high will depend on the previous state, the current modulation index, and the current data α_i. The previous state will inherently depend on all previous α but the circuit logic need only depend on the most previous state.

Using figure 20, the following Boolean equations are made:

$$
\begin{aligned}
A &= \bar{mi} \cdot B \cdot z^{-1} \\
B &= mi \cdot \left(D \cdot z^{-1} \cdot \Psi_1 + H \cdot z^{-1} \cdot \Psi_2\right) \\
C &= mi \cdot \left(A \cdot z^{-1} \cdot \Psi_1 + E \cdot z^{-1} \cdot \Psi_2\right) \\
D &= \bar{mi} \cdot G \cdot z^{-1} \\
E &= \bar{mi} \cdot F \cdot z^{-1} \\
F &= mi \cdot \left(D \cdot z^{-1} \cdot \Psi_2 + H \cdot z^{-1} \cdot \Psi_1\right)
\end{aligned}
\tag{13}
$$

The set of all waveforms for -f and +f of the MSK format.

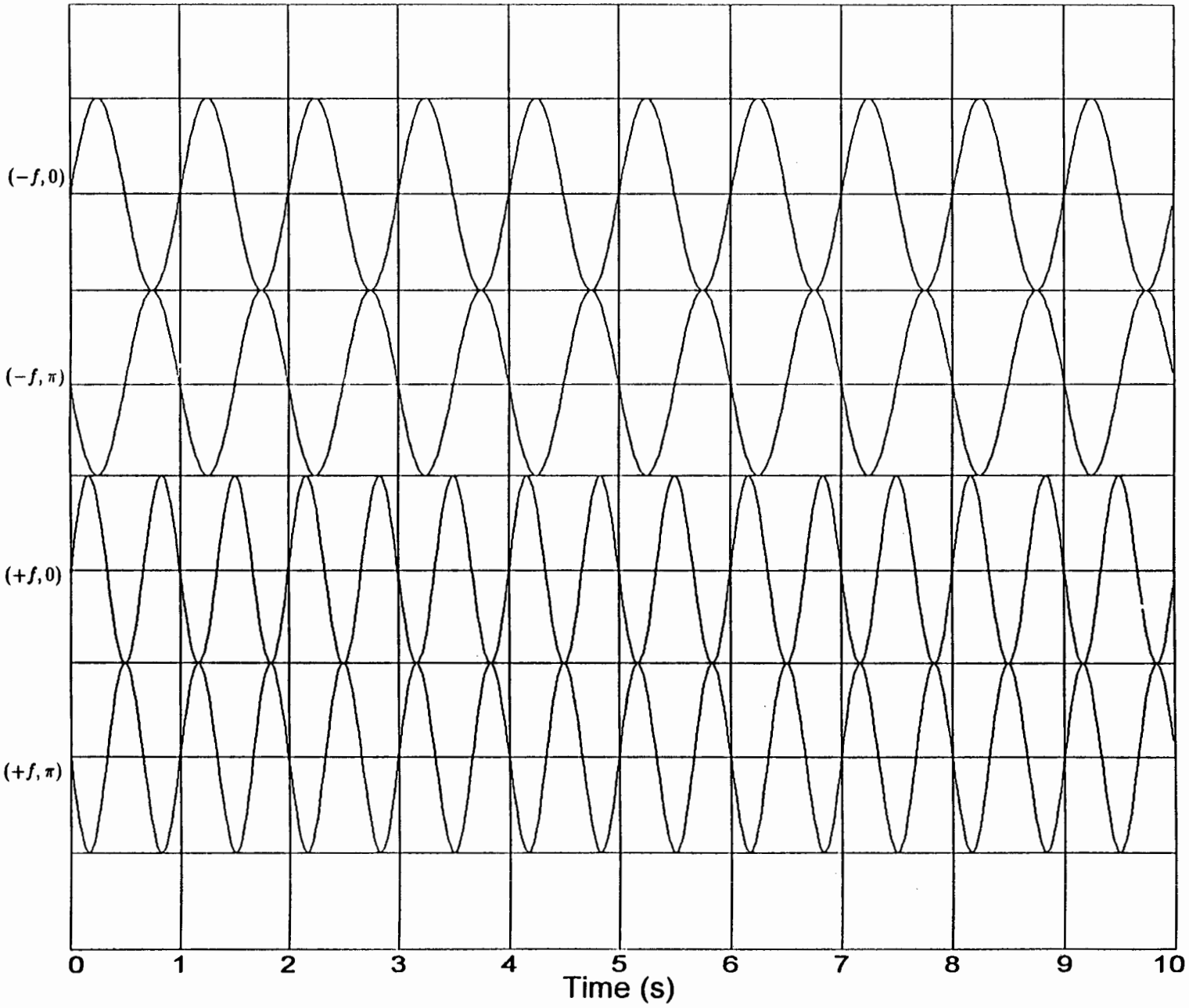

PROJECT

Figure 15

TITLE

OPERATOR

Page 49 7/1/94

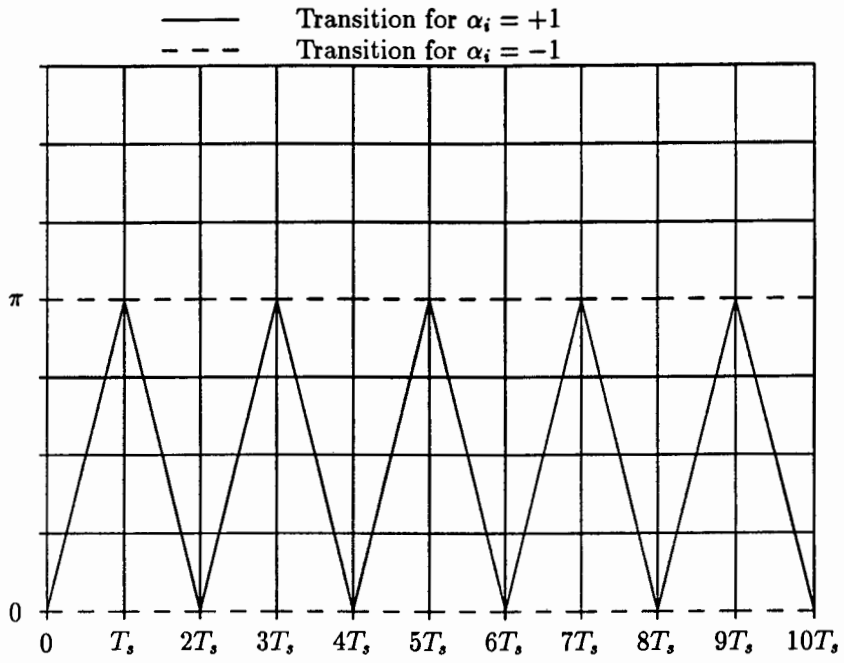

Figure 16: A multi-oscillator phase trellis of MSK.

$$G = mi \cdot \left(A \cdot z^{-1} \cdot \Psi_2 + E \cdot z^{-1} \cdot \Psi_1\right)$$

$$H = \bar{mi} \cdot C \cdot z^{-1}$$

$$a = A + B$$

$$b = C + D$$

$$c = E + F$$

$$d = G + H$$

where:

$$\Psi_1 = d \cdot z^{-1} \cdot \bar{d} + \bar{d} \cdot z^{-1} \cdot d$$

$$\Psi_2 = d \cdot z^{-1} \cdot d + \bar{d} \cdot z^{-1} \cdot \bar{d}$$

$$mi = \begin{cases} 0 \text{ (low)}, & \text{for } h_1 \\ 1 \text{ (high)}, & \text{for } h_2 \end{cases}$$

$\bar{d}$: binary 0 (low)

d : binary 1 (high)

z^{-1} : Delay operator (i.e. represents the previous symbol-interval)

A circuit representation of equation set 13, with additional simplification by De Morgan's Theorem, is shown in figure 22.

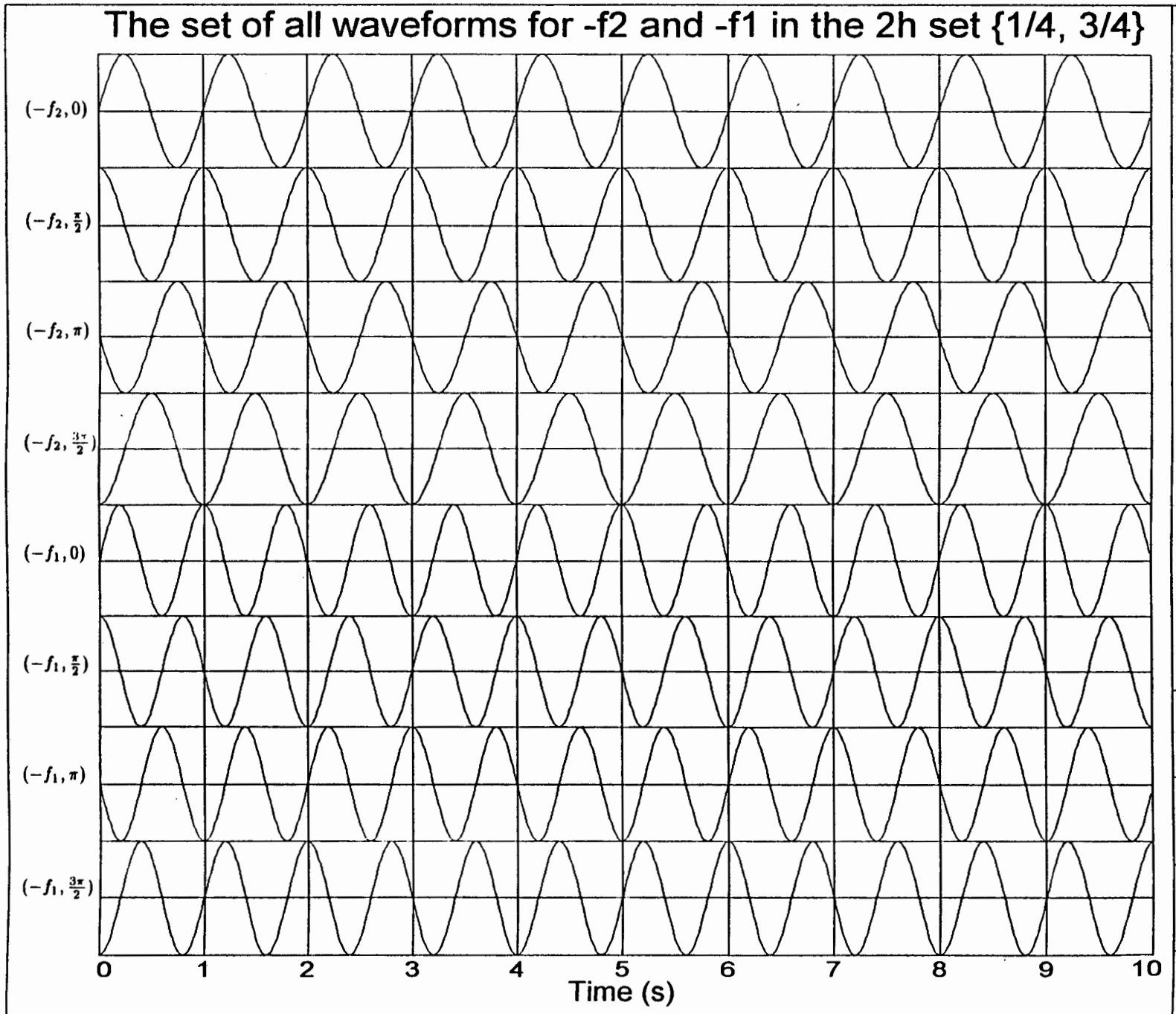

PROJECT

Figure 17

TITLE

OPERATOR

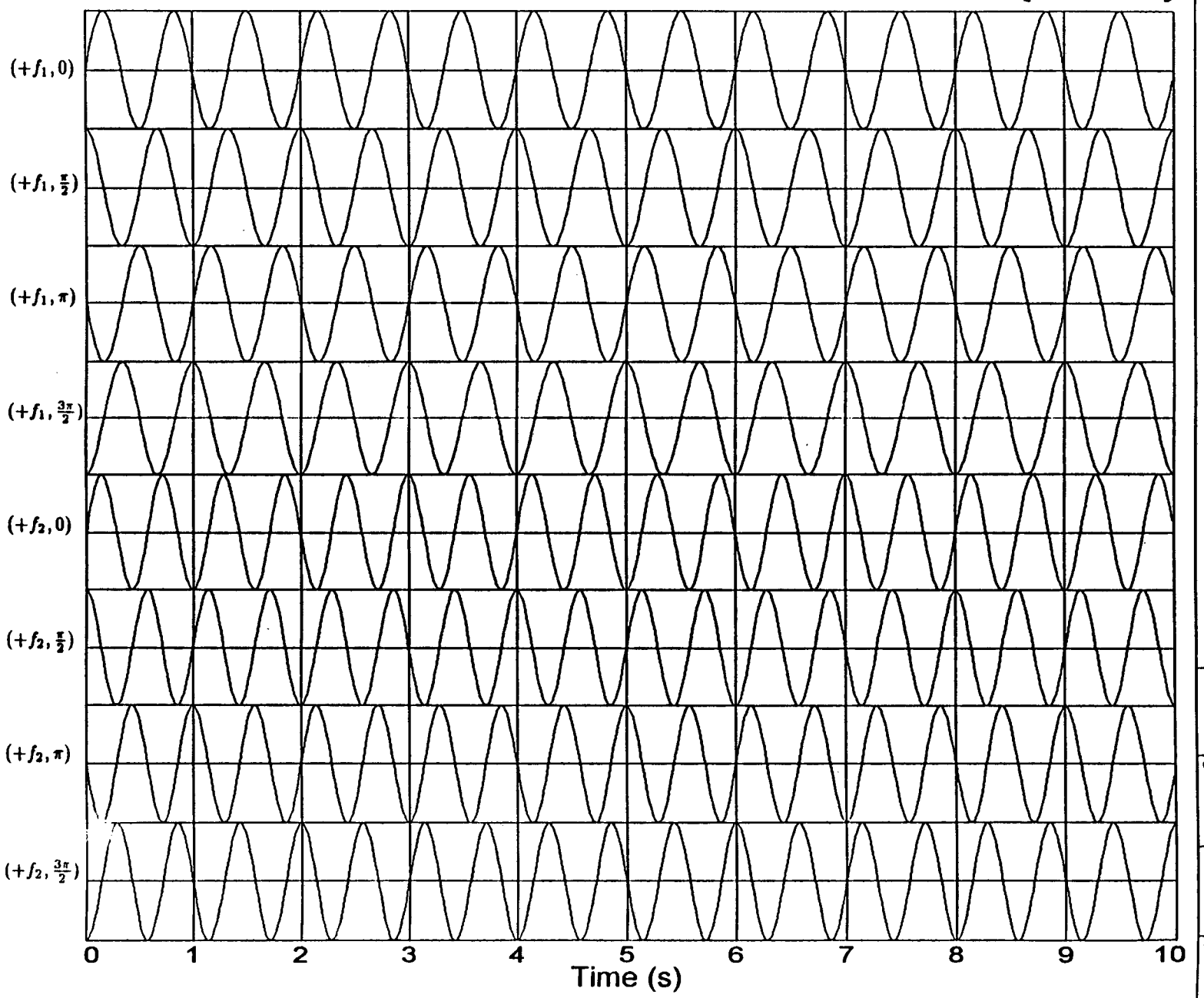

PROJECT

Figure 18

TITLE

OPERATOR

Page 52 7/1/94

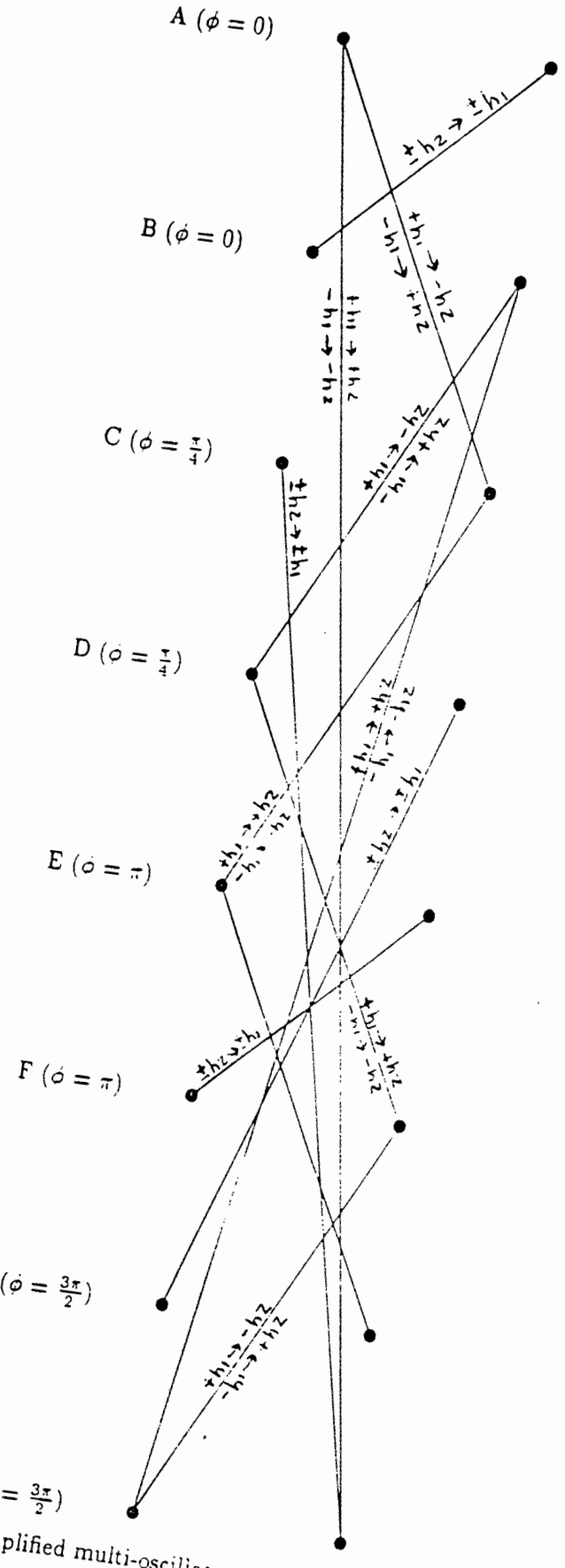

Figure 20: A simplified multi-oscilliator phase trellis for the 2-h set $\{\frac{1}{4}, \frac{3}{4}\}$

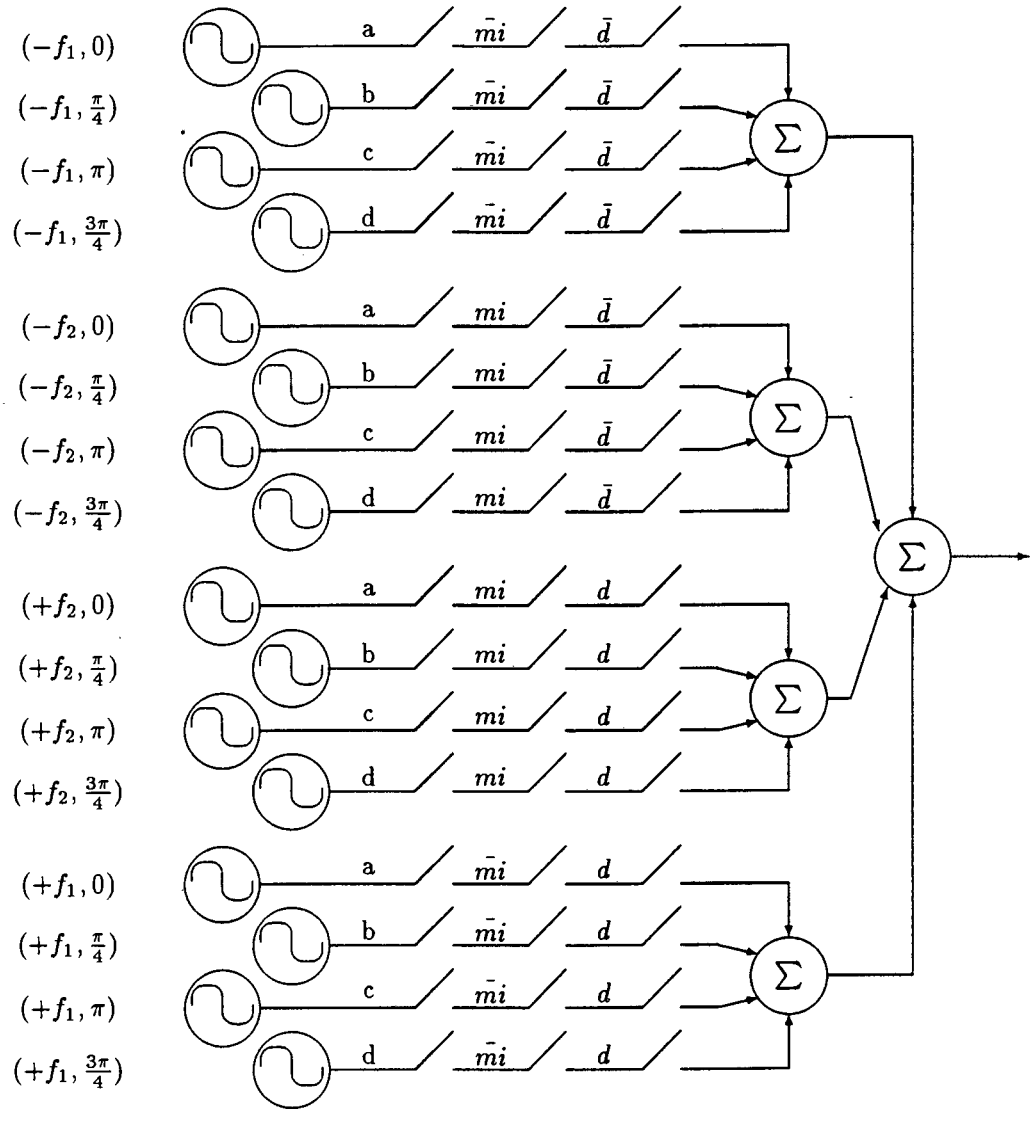

Figure 21: A multi-oscillator 2-h modulator for the set $H_2 = \{\frac{1}{4}, \frac{3}{4}\}$.

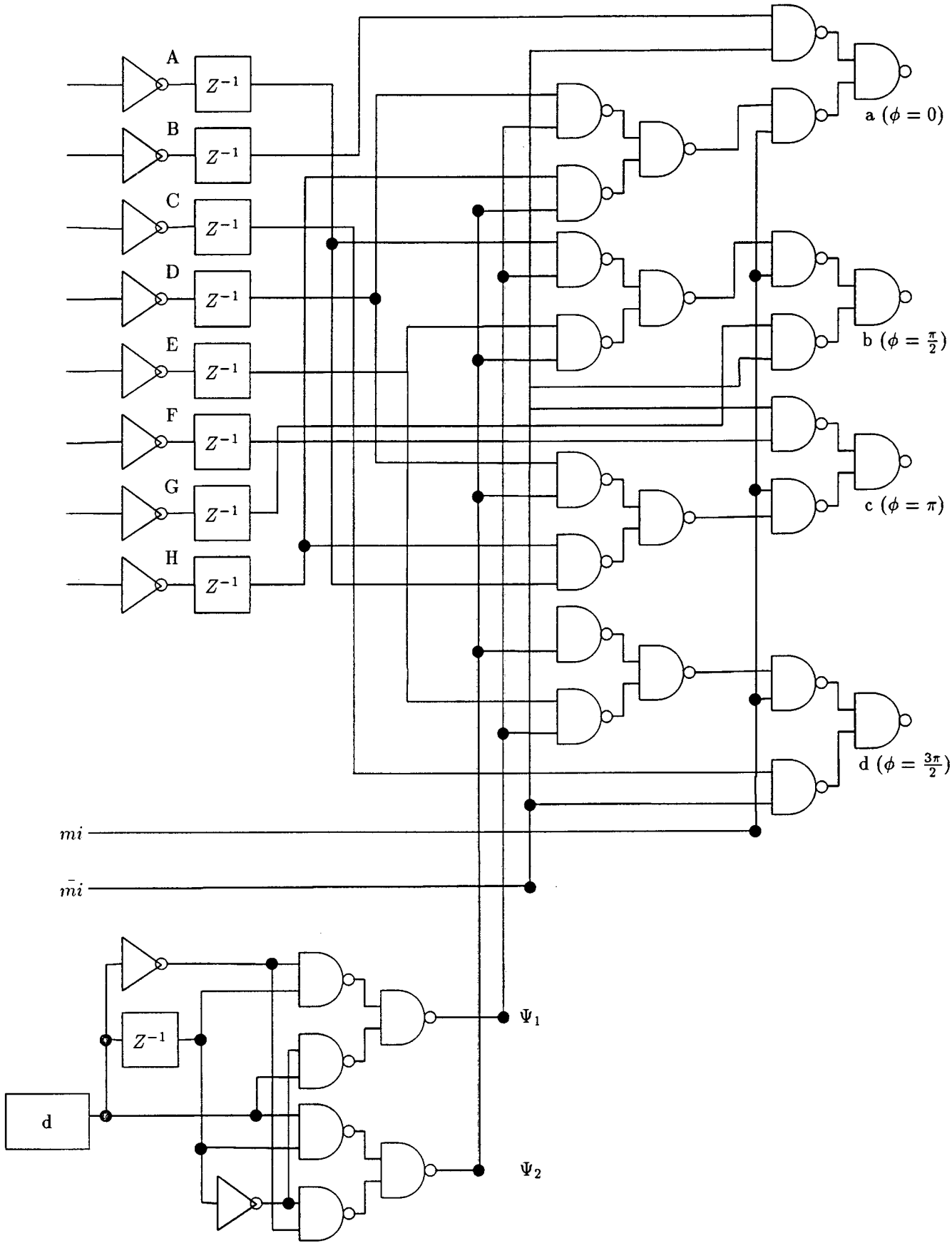

Figure 22: Logic representation of a binary coder for a multi-oscillator 2-h modulator for the set $H_2 = \{\frac{1}{4}, \frac{3}{4}\}$.

5.5 Multi-Oscillator Implementation for the Set $H_2 = \{\frac{1}{4}, \frac{2}{4}\}$

For a full constraint length code $H_2 = \{\frac{1}{4}, \frac{2}{4}\}$, the number of phase states increases considerably:

$$
\begin{array}{cccc}
(-\Delta f_1, 0) & (-\Delta f_1, 0) & (-\Delta f_1, 0) & (-\Delta f_1, 0) \\
(-\Delta f_1, \frac{\pi}{4}) & (-\Delta f_1, \frac{\pi}{4}) & (-\Delta f_1, \frac{\pi}{4}) & (-\Delta f_1, \frac{\pi}{4}) \\
(-\Delta f_1, \frac{\pi}{2}) & (-\Delta f_1, \frac{\pi}{2}) & (-\Delta f_1, \frac{\pi}{2}) & (-\Delta f_1, \frac{\pi}{2}) \\
(-\Delta f_1, \frac{3\pi}{4}) & (-\Delta f_1, \frac{3\pi}{4}) & (-\Delta f_1, \frac{3\pi}{4}) & (-\Delta f_1, \frac{3\pi}{4}) \\
(-\Delta f_1, \pi) & (-\Delta f_1, \pi) & (-\Delta f_1, \pi) & (-\Delta f_1, \pi) \\
(-\Delta f_1, \frac{5\pi}{4}) & (-\Delta f_1, \frac{5\pi}{4}) & (-\Delta f_1, \frac{5\pi}{4}) & (-\Delta f_1, \frac{5\pi}{4}) \\
(-\Delta f_1, \frac{3\pi}{2}) & (-\Delta f_1, \frac{3\pi}{2}) & (-\Delta f_1, \frac{3\pi}{2}) & (-\Delta f_1, \frac{3\pi}{2}) \\
(-\Delta f_1, \frac{7\pi}{4}) & (-\Delta f_1, \frac{7\pi}{4}) & (-\Delta f_1, \frac{7\pi}{4}) & (-\Delta f_1, \frac{7\pi}{4})
\end{array}
$$

The waveform of each sinusoid associated with this set is shown in figures 23, 24, 25, and 26. Using the method described previously, the multi-oscillator phase trellis similar to figure 19 is shown for the set $H_2 = \{\frac{1}{4}, \frac{2}{4}\}$ in figure 27. The circuit implementation and simplified trellis is not presented due to it's prohibitive complexity and size. The corresponding Boolean equations are shown in equation 14.

$$
\begin{aligned}
A &= \bar{mi} \cdot Dz^{-1} \\
B &= mi \cdot (Fz^{-1}\Upsilon_3 + Nz^{-1} \cdot \Upsilon_1 + Vz^{-1} \cdot \Upsilon_4 + [AD]z^{-1} \cdot \Upsilon_2) \\
C &= \bar{mi} \cdot Rz^{-1} \\
D &= mi \cdot (Hz^{-1}\Upsilon_4 + Pz^{-1} \cdot \Upsilon_2 + Xz^{-1} \cdot \Upsilon_3 + [AF]z^{-1} \cdot \Upsilon_1) \\
E &= mi \cdot (Az^{-1}\Upsilon_4 + Iz^{-1} \cdot \Upsilon_2 + Qz^{-1} \cdot \Upsilon_3 + Yz^{-1} \cdot \Upsilon_1) \\
F &= \bar{mi} \cdot (Mz^{-1} \cdot \bar{d} + [AC]z^{-1} \cdot d) \\
G &= \bar{mi} \cdot (Cz^{-1}\Upsilon_3 + Kz^{-1} \cdot \Upsilon_2 + Sz^{-1} \cdot \Upsilon_4 + [AA]z^{-1} \cdot \Upsilon_3) \\
H &= \bar{mi} \cdot (Oz^{-1} \cdot d + [AE]z^{-1} \cdot \bar{d}) \\
I &= \bar{mi} \cdot Lz^{-1} \\
J &= mi \cdot (Fz^{-1}\Upsilon_2 + Nz^{-1} \cdot \Upsilon_3 + Vz^{-1} \cdot \Upsilon_4 + [AD]z^{-1} \cdot \Upsilon_2) \\
K &= \bar{mi} \cdot Zz^{-1} \\
L &= mi \cdot (Hz^{-1}\Upsilon_1 + Pz^{-1} \cdot \Upsilon_4 + Xz^{-1} \cdot \Upsilon_2 + [AA]z^{-1} \cdot \Upsilon_3) \\
M &= mi \cdot (Az^{-1}\Upsilon_2 + Iz^{-1} \cdot \Upsilon_4 + Qz^{-1} \cdot \Upsilon_1 + [AA]z^{-1} \cdot \Upsilon_3) \\
N &= \bar{mi} \cdot (Ez^{-1} \cdot d + Uz^{-1} \cdot \bar{d}) \\
O &= mi \cdot (Cz^{-1}\Upsilon_1 + Kz^{-1} \cdot \Upsilon_3 + Sz^{-1} \cdot \Upsilon_2 + [AA]z^{-1} \cdot \Upsilon_4) \\
P &= \bar{mi} \cdot (Gz^{-1} \cdot \bar{d} + Wz^{-1} \cdot d)
\end{aligned}
\tag{14}
$$

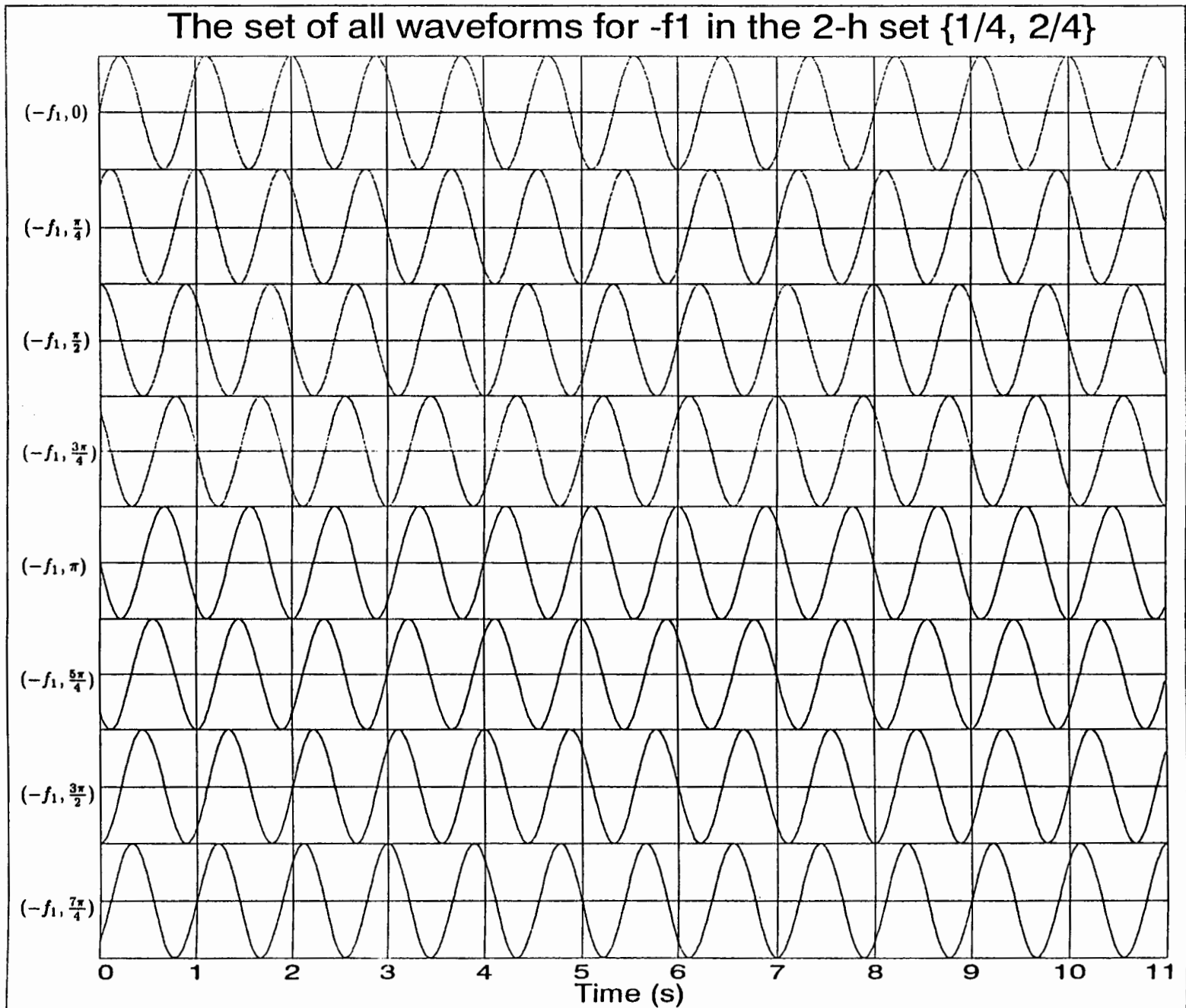

PROJECT

Figure 23

TITLE

OPERATOR

Page 58 7/1/94

SIMULINK

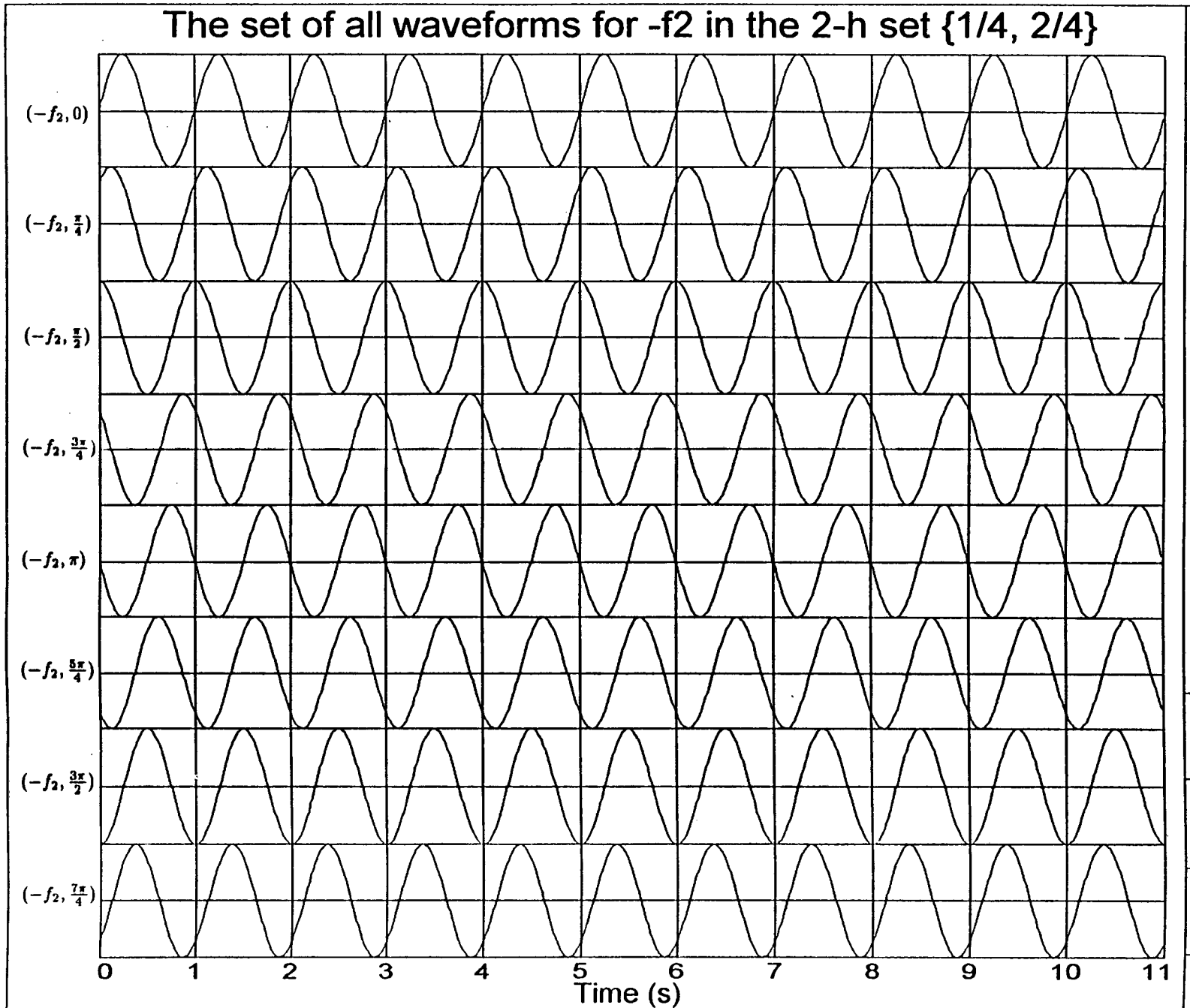

PROJECT

Figure 24

TITLE

OPERATOR

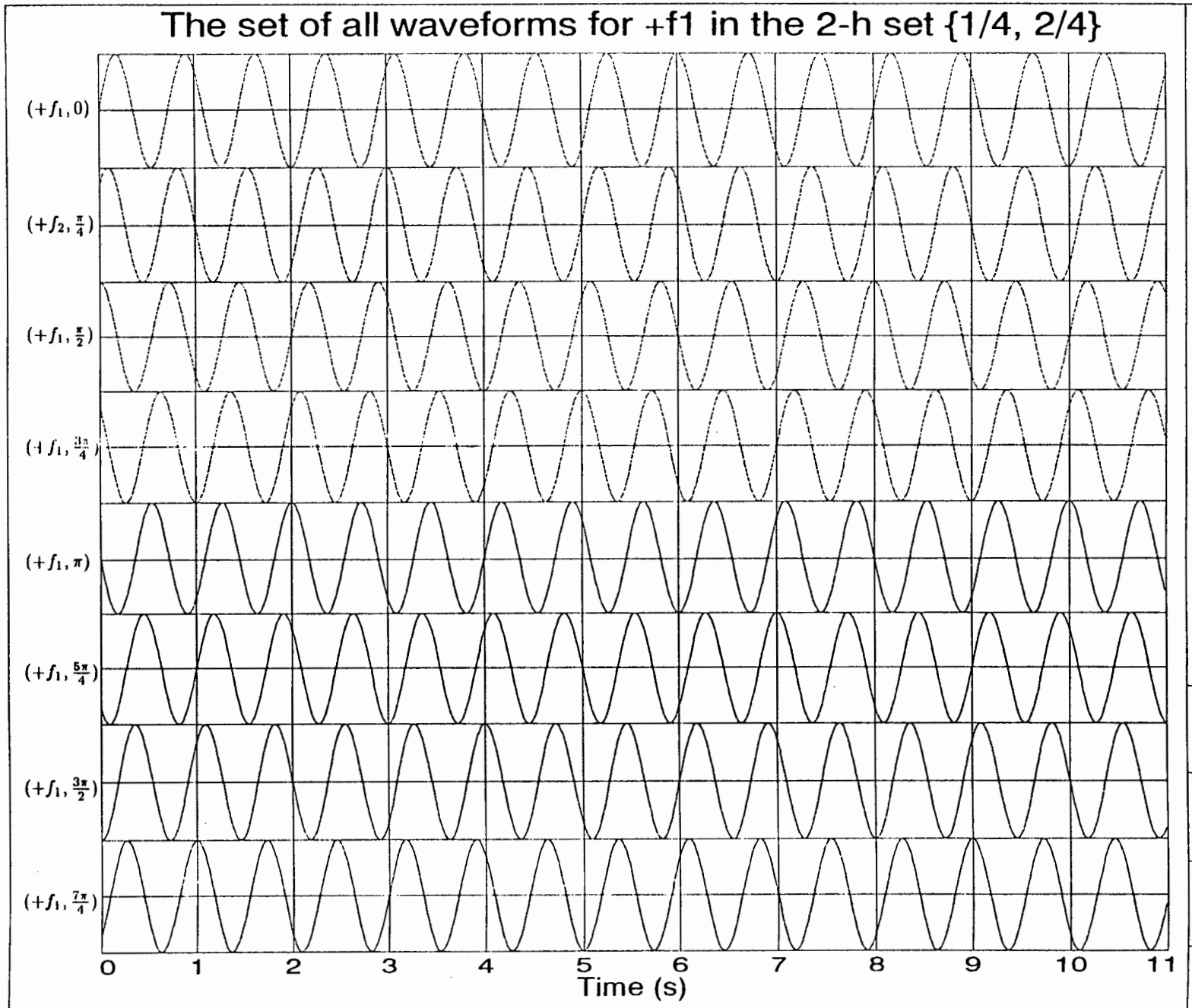

PROJECT

Figure 25

TITLE

OPERATOR

Page 60 7/1/94

NIMA PLANTS

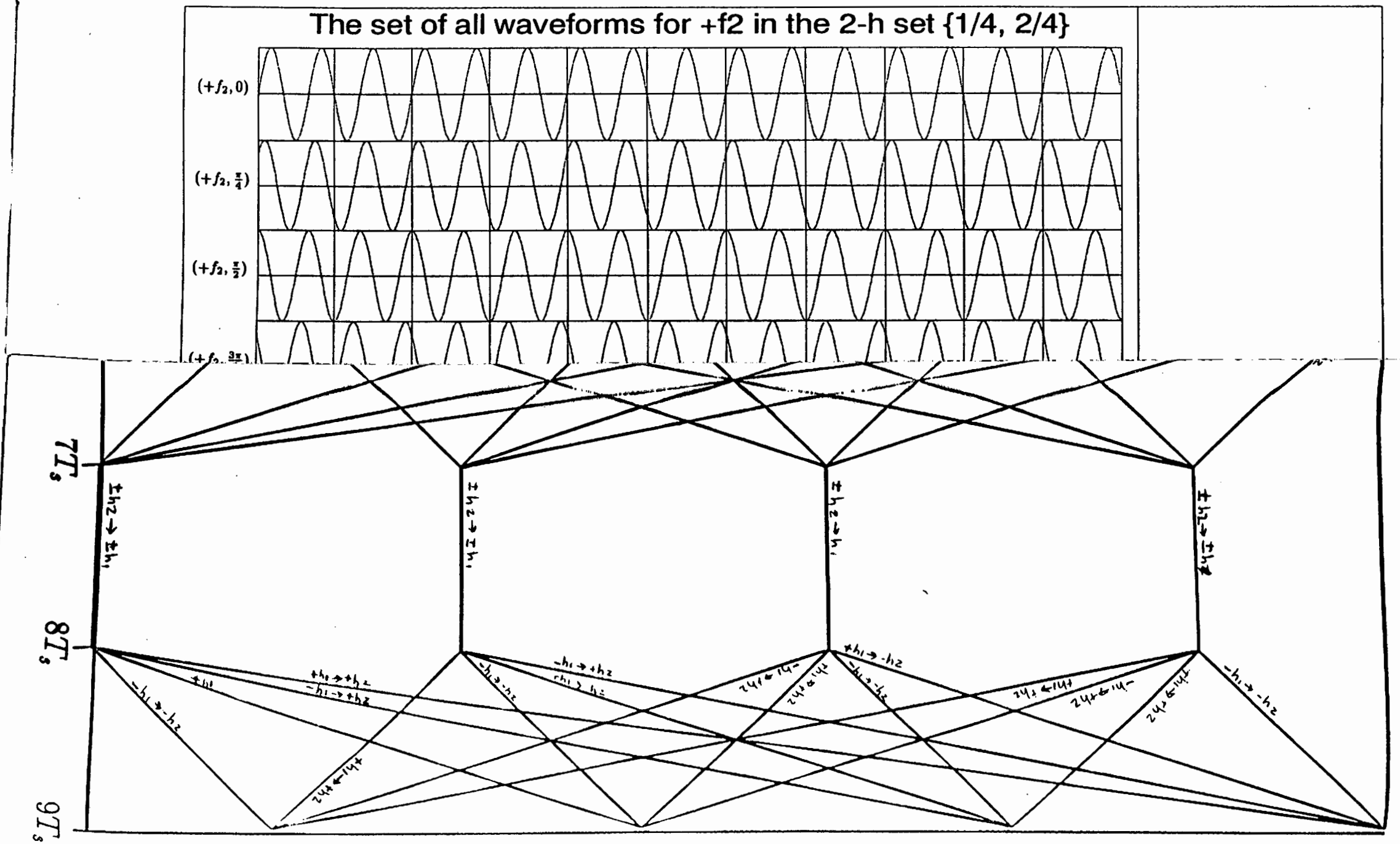
The set of all waveforms for +f2 in the 2-h set {1/4, 2/4}
$(+f_2, 0)$
$(+f_2, \frac{\pi}{4})$
$(+f_2, \frac{\pi}{2})$
$(+f_2, \frac{3\pi}{4})$
π/s
$8\pi/s$
$16\pi/s$
$\pm h_1 \rightarrow \pm h_2$
$\pm h_2 \rightarrow \pm h_1$
$\pm h_1 \rightarrow \pm h_2$
$\pm h_2 \rightarrow \pm h_1$
$+h_1 \rightarrow +h_2$
$-h_1 \rightarrow +h_2$
$+h_1 \rightarrow -h_2$
$-h_1 \rightarrow -h_2$
$2\pi \leftarrow 14\pi$

$$Q = \bar{mi} \cdot Tz^{-1}$$

$$R = mi \cdot \left(Fz^{-1}\Upsilon_4 + Nz^{-1} \cdot \Upsilon_2 + Vz^{-1} \cdot \Upsilon_3 + [AD]z^{-1} \cdot \Upsilon_1\right)$$

$$S = mi \cdot Bz^{-1}$$

$$T = mi \cdot \left(Hz^{-1}\Upsilon_3 + Pz^{-1} \cdot \Upsilon_1 + Xz^{-1} \cdot \Upsilon_4 + [AF]z^{-1} \cdot \Upsilon_2\right)$$

$$U = mi \cdot \left(Fz^{-1}\Upsilon_2 + Nz^{-1} \cdot \Upsilon_3 + Vz^{-1} \cdot \Upsilon_4 + [AD]z^{-1} \cdot \Upsilon_2\right)$$

$$X = \bar{mi} \cdot \left(Oz^{-1} \cdot \bar{d} + [AE]z^{-1} \cdot d\right)$$

$$Y = \bar{mi} \cdot [AB]z^{-1}$$

$$Z = mi \cdot \left(Fz^{-1}\Upsilon_1 + Nz^{-1} \cdot \Upsilon_4 + Vz^{-1} \cdot \Upsilon_2 + [AD]z^{-1} \cdot \Upsilon_3\right)$$

$$[AA] = mi \cdot Jz^{-1}$$

$$[AB] = mi \cdot \left(Hz^{-1}\Upsilon_2 + Pz^{-1} \cdot \Upsilon_3 + Xz^{-1} \cdot \Upsilon_1 + [AF]z^{-1} \cdot \Upsilon_4\right)$$

$$[AC] = mi \cdot \left(Az^{-1}\Upsilon_1 + Iz^{-1} \cdot \Upsilon_3 + Qz^{-1} \cdot \Upsilon_2 + Yz^{-1} \cdot \Upsilon_4\right)$$

$$[AD] = \bar{mi} \cdot \left(Ez^{-1} \cdot \bar{d} + Uz^{-1} \cdot d\right)$$

$$[AE] = mi \cdot \left(Cz^{-1}\Upsilon_2 + Kz^{-1} \cdot \Upsilon_4 + Sz^{-1} \cdot \Upsilon_1 + [AA]z^{-1} \cdot \Upsilon_3\right)$$

$$[AF] = \bar{mi} \cdot \left(Gz^{-1} \cdot d + Wz^{-1} \cdot \bar{d}\right)$$

where:

$$\Upsilon_1 = d \cdot z^{-1} \cdot d$$

$$\Upsilon_2 = d \cdot z^{-1} \cdot \bar{d}$$

$$\Upsilon_3 = \bar{d} \cdot z^{-1} \cdot d$$

$$\Upsilon_4 = \bar{d} \cdot z^{-1} \cdot \bar{d}$$

This exercise demonstrates the nature of the multi-oscillator modulator using a binary transducer, as well as the rapid increase of the complexity with the number of signal states, qKM. It can be seen here that a ternary form of a transducer would lead to significant simplifications in the structure.

6 Receiver Structures

6.1 The Maximum Likelihood Detection (MLHD) of Multi-h Coded Modulation

6.1.1 Signal Space Representation

The theory of Maximum Likelihood Detection is modified for Multi-h coding. In general, the modulated signal is considered a vector [3]:

$$\begin{aligned} s_i &= \begin{bmatrix} s_{i1} \\ s_{i2} \\ s_{i3} \\ \vdots \\ s_{iN} \end{bmatrix} && \text{i=1,2,..,M} \\ &= \textstyle\sum_{j=1}^{N} s_{ij}\phi_j(t) && iT_s \le t \le (i+1)T_2 \\ & && i = 1, 2, \ldots, M \end{aligned} \tag{15}$$

where:

$$\begin{aligned} s_{ij} &= \textstyle\int_{iT_s}^{(i+1)T_s} s_i(t)\phi_j(t)dt && i = 1, 2, \ldots, M \\ & && j = 1, 2, \ldots, N \end{aligned}$$

$$E_i = \textstyle\int_0^{T_s} s_i^2(t)dt \qquad i = 1, 2, \ldots, M \text{(signal energy)}$$

In equation 15, M=number of signal points, N=number of orthonormal basis functions$\phi_i(t)$. The signal space diagram for coherent binary FSK is shown in figure 28. Note that for FSK, N=M, since there is a basis function for each signal frequency. For a set of orthonormal basis functions, with the bit energy normalized to one:

$$\int_{iT_s}^{(i+1)T_s} \phi_i\phi_j = \begin{cases} 1 & \text{if i=j} \\ 0 & \text{if i} \neq \text{j} \end{cases}$$

For this modulation type:

$$s_i(t) = \begin{cases} \sqrt{\frac{2E_b}{T_b}}cos(2\pi f_i t) & iT_s \le t \le (i+1)T_s \\ 0 & elsewhere \end{cases}$$

$$\phi_i(t) = \begin{cases} \sqrt{\frac{2}{T_b}}cos(2\pi f_i t) & iT_s \le t \le (i+1)T_s \\ 0 & elsewhere \end{cases}$$

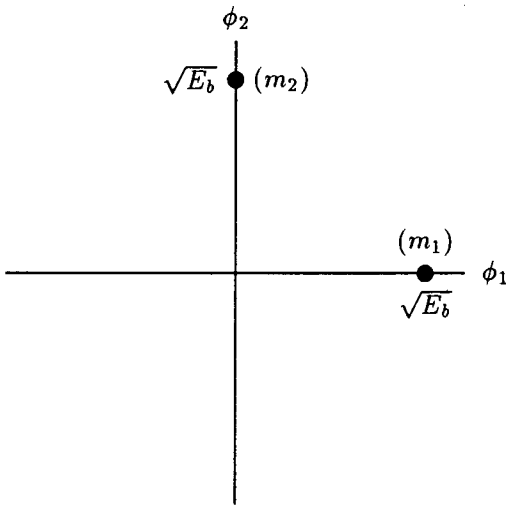

Figure 28: Signal space diagram for coherent binary FSK system.

Then:

$$s_1 = \begin{bmatrix} \sqrt{E_b} \\ 0 \end{bmatrix}$$

$$s_2 = \begin{bmatrix} 0 \\ \sqrt{E_b} \end{bmatrix}$$

Because the only difference between generalized FSK and CPFSK is a continuous-phase constraint, the signal space diagram given here also applies to the continuous phase case. Let:

$$\bar{r} = s(\phi_i, \alpha_i) + \bar{n}$$

where $\bar{n}$ is a vector of independent Gaussian random variables with zero mean and variance of $\frac{N_o}{2}$. $s(t, \bar{\alpha})$ is that defined previously for CPFSK. In an additive white Gaussian channel, the vector form of the signal at the receiver is a random variable X:

$$\begin{aligned} X(t) &= \sum_{j=1}^{N} X_j \phi_j(t) + W(t) \\ &= \begin{bmatrix} X_1 \\ X_2 \\ \vdots \\ X_N \end{bmatrix} \\ X_j &= \int_{iT_s}^{(i+1)T_s} X(t)\phi_j(t)dt \\ &= s_{ij} + W_j \qquad\qquad j = 1, 2, \ldots, N \end{aligned}$$

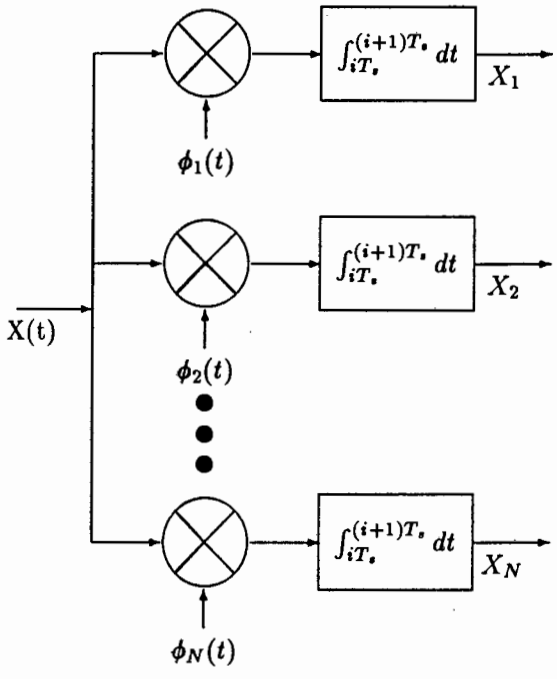

Figure 29: Output of a set of receiver correlators.

where X_j is the random signal for each set of correlator outputs shown in figure 29, W(t) is AWGN channel and receiver noise combined into one term. This is permissible since both types of noise are additive.

6.1.2 Basis and Likelihood Functions for Multi-h Coded CPFSK

For the multi-h coded signal, there exists a partitioned set of N total basis functions for each of the signals. This set is partitioned K subsets of N' points each. There are then M basis functions for each modulation index: $\pm sin(\omega_o \pm \frac{Ah_i}{2T_s})$, where $A = \{\pm 1, \pm 3, \ldots, \pm(M-1)\}$. In figure 30, the entire set of N signal points are shown distributed over the super-interval T'=KT. For the assumption that N=M for a set H_K of size K with M signaling levels, there will be $N = \frac{KM}{K}$ or M basis functions for each bit period. This means that because only M correlators are switched into the circuit output, the output of the correlators gathered and compared in the same manner as with the coherent FSK receiver. For the AWGN channel, the generalized likelihood function is:

$$f_{\bar{X}}(\bar{X}|m_i) = (\pi N_o)^{-N/2} e^{-\frac{1}{N_o}\sum_{j=1}^{N}(x_j - s_{ij})^2} \quad \text{i=1,2,}\cdots\text{,M}$$

For Multi-h signalling, this expression is of the form:

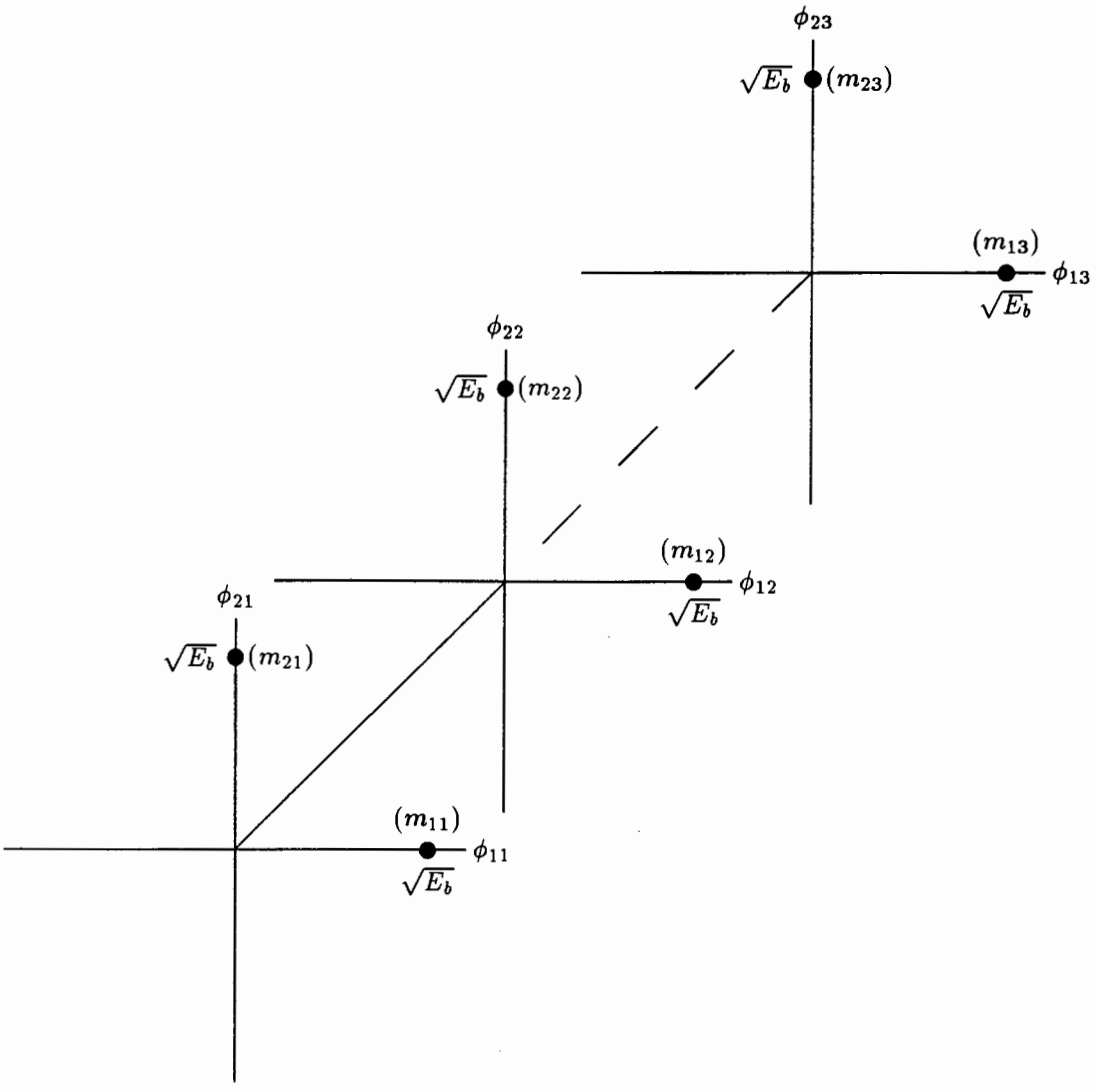

Figure 30: Partitioned signal space of multi-h coded CPFSK.

$$f_{\bar{X}_k}(\bar{X}_k|m_{ik}) \quad = \quad (\pi N_o)^{-N/2} e^{-\frac{1}{N_o}\sum_{j=1}^{M}(x_{ij}-s_{ikj})^2} \qquad \text{i=1,2,}\cdots\text{,M}$$

where $k = 1, 2, \cdots, K$, $i = 1, \cdots, M$, and $j = 1, \cdots, N = M$.

6.2 A Receiver Simulation: The Effects of Signal Frequency Variations on Bit-Error Performance

With this theory of MLHD of Multi-H CPFSK signals in mind, it was of particular interest in this research to quantify the effect of signal-frequency variations of non-linear modulators on the MLHD process in the presence of noise. A switched bank of correlators, one for each h_i, is assumed here as

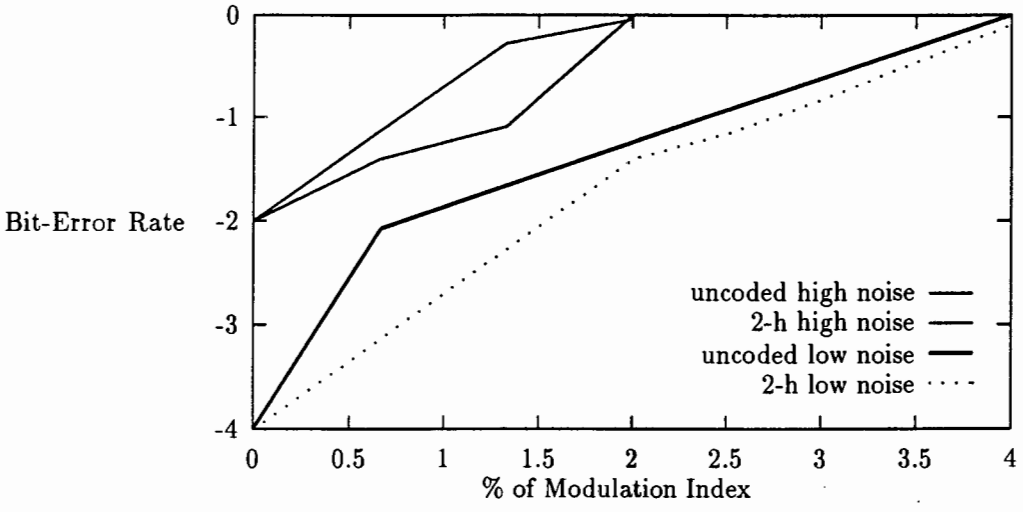

Figure 31: Comparison of Measured Bit-error Rate performance for uncoded and Multi-h coded CPFSK

well as MK total signals in the signal set and N=MK total basis functions is used for the entire set H_K.

It is desired to know how the bit-error characteristics of MLHD for the partitioned signal constellation for each h_i compares with the uncoded case as one signal point in the constellation is varied in frequency. Uncoded binary CPFSK signal was compared with a coded binary CPFSK signal using a 2-H set $\{\frac{1}{4}, \frac{2}{4}\}$.

Of particular interest was the whether a threshold existed which would permit wider tolerance of variations of a signal frequency while maintaining an exceptable level of bit-error performance. A simulation was developed with a switched bank of correlators, utilizing oscillator-multiplier stages followed by a sampled integrate-and-dump. A signal frequency at the modulator was varied while keeping the channel noise constant. This result is shown in figure 31. The overall bit-error performance curve of the coded signal for each frequency offset is shown in figure 32.

As expected, bit-error performance degraded for $\Delta f > 0$ and was found worse for higher channel noise. For large frequency variations, figure 32 shows little improvement in bit-error performance for $\frac{E_b}{N_o} > 16dB$.

For the coded case, however, the bit-error rate did not degrade as rapidly for small variations of Δf. In all cases, the noise became prohibitive for a signalling variation of only 4% of h. The effect of non-linear frequency variation at the modulator will typically occur for more than one signal point. It will also vary differently for each signal point due to non-linearity of the modulator. The error, therefore, will be much more pronounced over the entire constellation.

There is little further to be gained in this regard by using higher orders of coding since the modest

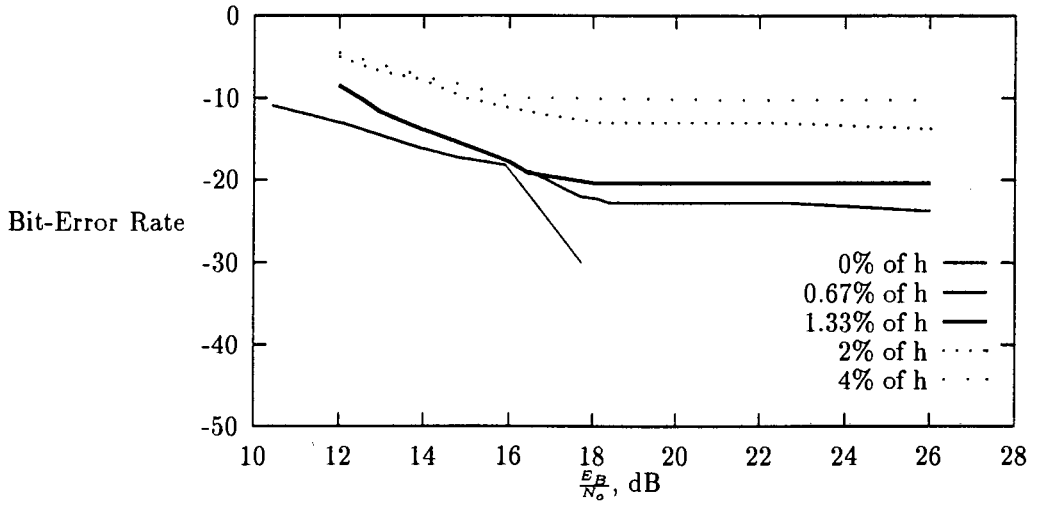

Figure 32: Bit-error deterioration of Multi-h coded CPFSK for $\Delta f > 0$.

gains available are not realized for variations as little as a few percent of the modulation index. These results quantitatively show the need for a high degree of linearity at the modulator in the case of coded, coherent CPFSK.

A non-ideal receiver structure has been presented [8] based on simplifications to the synchronization circuit. While carrier reconstruction is not a topic of this work, it is beneficial to consider this structure briefly. It is pointed out here that an important reason for receiver complexity is that of carrier recovery.

The strategy of this simplification is to modify the approach to synchronization such that a cycled bank of matched filters is not needed. This would be replaced by a single set of filters matched to the average modulation index, h_{avg}. According to simulation results of Premji, the coding degradation is surprisingly only a fraction of a decibel. Since good, full constraint length codes tend to fall closely to the h_{avg} (i.e. small standard deviation s^2), this type of non-ideal MLHD is best suited for such codes.

7 Conclusions

- **This work began with a complete mathematical description of Multi-h coded CPFSK signals has been presented, including the motivation of it's application.** The derivation of methods for determining spectral and bit-error performance of these codes has also been shown. The direct method has been chosen as the most accurate form of Power Density determination. It is also the most descriptive for this coding method because it can be calculated as an explicit function of the modulation indices used. The mathematical characteristics of error probabilities with respect to the set H_K have also been explained. The resulting improvements to standard performance criteria are also provided. By considering an ensemble average over a super-interval $T' = KT$ it has been shown that the piecewise description of these coded signals is similar to uncoded CPFSK.

- **Criteria for the selection of Multi-h code sets with favourable performance has been established from this research.** The maximum constraint codes merge in K+1 intervals, where K is the number of indices in the set. Methods for the determination of code sets which maintain this constraint length has been given.

- **It has been found that the implementation of this method is simpler than for data coding since no memory or shift registers are required for the modulator.** Only a clock circuit to switch the modulation indices is needed. In the case of a single oscillator VCO, minor modifications to the DC level shifter used to drive the VCO would be made to accommodate the generation of the Markov chain. In this case, the VCO would inherently maintain continuous phase and memory is not needed. In the case of the multi-oscillator structure, the memory for phase is maintained in the coder.

- **A multi-oscillator form of the phase trellis diagram has also been developed.** This trellis follows the phase states with respect to the current signal frequency $f = f_o \pm \frac{h_i}{2T_s}$ instead of f_o. This form of phase trellis has been found useful for determining Markov chain of signal states of a given code set H_K. It has also been found that full constraint length codes also contain a relatively high number of signal states which must be resolved, as compared to non-optimum constraint length code sets.

- **This multi-oscillator trellis also has been used to determine a state machine as a switching network for a bank of oscillators.** There is an oscillator at every signaling frequency and phase for all signal states in the set H_K. The switching network is used to switch one oscillator to the output at a time such that the output is always phase continuous. This is structure is similar to the ternary coder given by Massey, except the transducer used here is a binary one.

- **A demodulator has been designed to determine the characteristics of Multi-h coded CPFSK in application.** It has been found that the decoding requirements are essentially the same as that for data coding. Constraint length decoding also requires an observation over an extended interval using minimum path calculation techniques such as Viterbi or Sequential decoding.

- **The signal space of Multi-h Coded CPFSK has been expressed as a partition of the conventional FSK representation.**For a switched bank of correlators, this means the decision regions are the same as that of the uncoded case.

- **It has been determined quantitatively that a modulator with a non-linear voltage-frequency characteristic is not suitable for coherent Multi-h CPFSK modulation.** This method of coded modulation requires a high degree of integrity for the signal frequencies. A deviation of only 4% of just one signal frequency results in a complete deterioration of bit-error performance.

7.1 Suggestions for Further Work

- **The Multi-T format presented may offer simplifications for DSP implementations since non-uniform symbol-periods may be more easily accommodated than multiple frequencies or potential increases in spectral occupation of multi-h coding.** It is recognized that multiple frequencies required by a multi-h format may also be just as easily generated by DSP. By using the comparable Multi-T format presented and choosing $R_{avg} = R_{mh}$, as defined previously, both formats are spectrally similar. In a comparative analysis, the small coding gains of Multi-T suggested by Holbowicz and Szulakiewicz would also be taken into account.

- **For the case of the multi-frequency modulator structure, a significant decrease in complexity could be made by the implementation of a ternary coder.** It is suggested this would take the form shown in figure 33. The number of oscillators has been reduced by a factor of two. Of what little is published on ternary coding [22] [23] [24], none is applicable in this regard. There is new work to be done with this type of ternary coding.

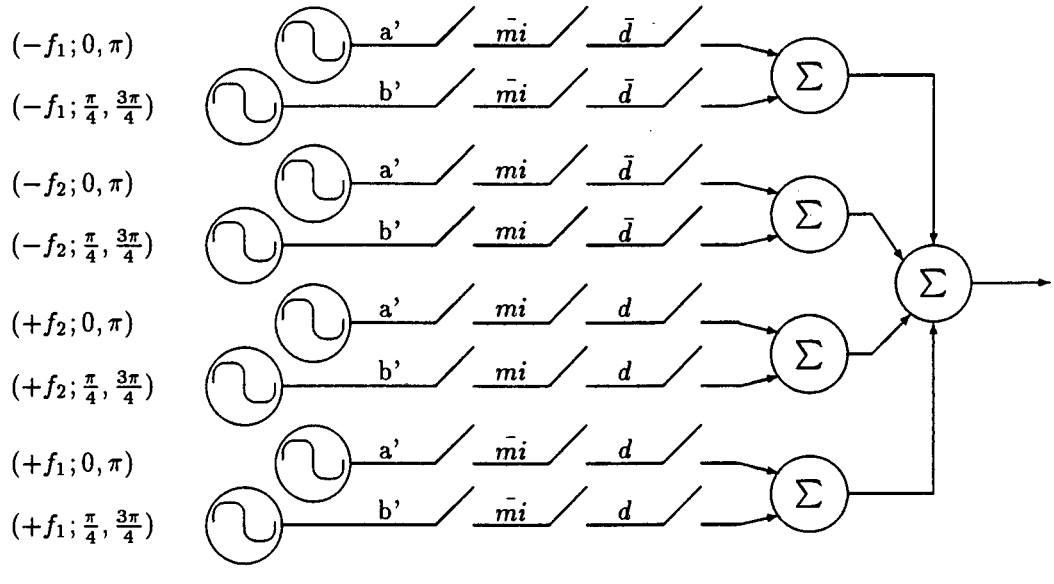

Figure 33: A typical structure for a ternary coded multi-h Massey modulator structure.

References

[1] Rodger E. Ziemer and Roger L. Peterson. *Introduction to Digital Communication.* Macmillan, 1992.

[2] S.O. Rice. Spectral density and autocorrelation functions associated with binary frequency-shift keying. *Bell System Technical Journal*, 42:2355–2385, September 1963.

[3] Simon Haykin. *Digital Communications.* John Wiley, 1988.

[4] Claude E. Shannon and Warren Weaver. *The Mathematical Theory of Communication.* University of Illinois Press, 1949.

[5] Rudi de Buda. Coherent demodulation of frequency-shift keying with low deviation ratio. *IEEE Transactions on Communications*, 20:429–435, June 1972.

[6] Peter J. McLane et. al. *Introduction to Trellis-Coded Modulation with Applications.* Macmillan Publishing, 1991.

[7] John B. Anderson and Desmon P. Taylor. A bandwidth-efficient class of signal-space codes. *IEEE Transactions on Information Theory*, 24:703–712, November 1978.

[8] Al-Nasir Premji. Receiver structures for m-ary multi-h phase codes. Technical Report CRL-186, McMaster University, January 1988.

[9] John P. Fonseka. Nonlinear continuous phase frequency shift keying. *IEEE Transactions on Communications*, 39:1473–1481, 1991.

[10] Witold Holubowicz and Pawel Szulakiewicz. Multi-$h$realization of multi-$h$phase codes. *IEEE Transaction on Information Theory*, 31:528–529, July 1985.

[11] Steven V. Pizzi and Stephen G. Wilson. Convolutional coding combined with continuous phase modulation. *IEEE Transactions on Communications*, 33(1):20–29, Jan 1987.

[12] Jr. G. David Forney. The viterbi algorithm. *Proceedings of the IEEE*, 61:265–278, March 1973.

[13] P. Galko and S. Pasupathy. The mean power spectral density of markov chain driven signals. *IEEE Transaction on Information Theory*, 27:746–756, November 1981.

[14] A.T. Lereim. Spectral properties of multi-h phase codes. Technical Report CRL-57, McMaster University, July 1978.

[15] Stephen G. Wilson and Richard C. Gaus. Power spectra of multi-$h$phase codes. *IEEE Transactions of Communications*, 29:250–256, March 1981.

[16] John B. Anderson et. al. *Digital Phase Modulation.* Plenum Press, 1986.

[17] J.E. Mazo and J. Salz. Spectra of frequency modulation with random waveforms. *Information Controls*, 9:414–422, 1966.

[18] S.O. Rice. Mathematical analysis of random noise. *Bell System Technical Journal*, 23:282–332, 1944.

[19] P. J. McLane et. al. A study on combined channel coding and modulation for mobile satellite communications. Technical report, McMaster University, March 1986.

[20] Cyrus Derman et. al. *A Guide to Probability Theory and Application.* Holt, Rinehart and Winston, 1973.

[21] James L. Massey. A generalized formulation of minimum shift keying modulation. *IEEE International Conference on Communications*, 2:26.5.1–26.5.4, June 1980.

[22] H. C. Ferreira. On ternary error correcting line codes. *IEEE Transactions on Communications*, 37:510–515, May 1989.

[23] W. Gary Huffman. On extremal self-dual ternary codes of lengths 28 to 40. *IEEE Transaction on Information Theory*, 38:1395–1400, July 1992.

[24] John F. Humphreys. Algebraic decoding of the ternary (13, 7, 5) quadratic residue code. *IEEE Transaction on Information Theory*, 38:1122–1125, May 1992.

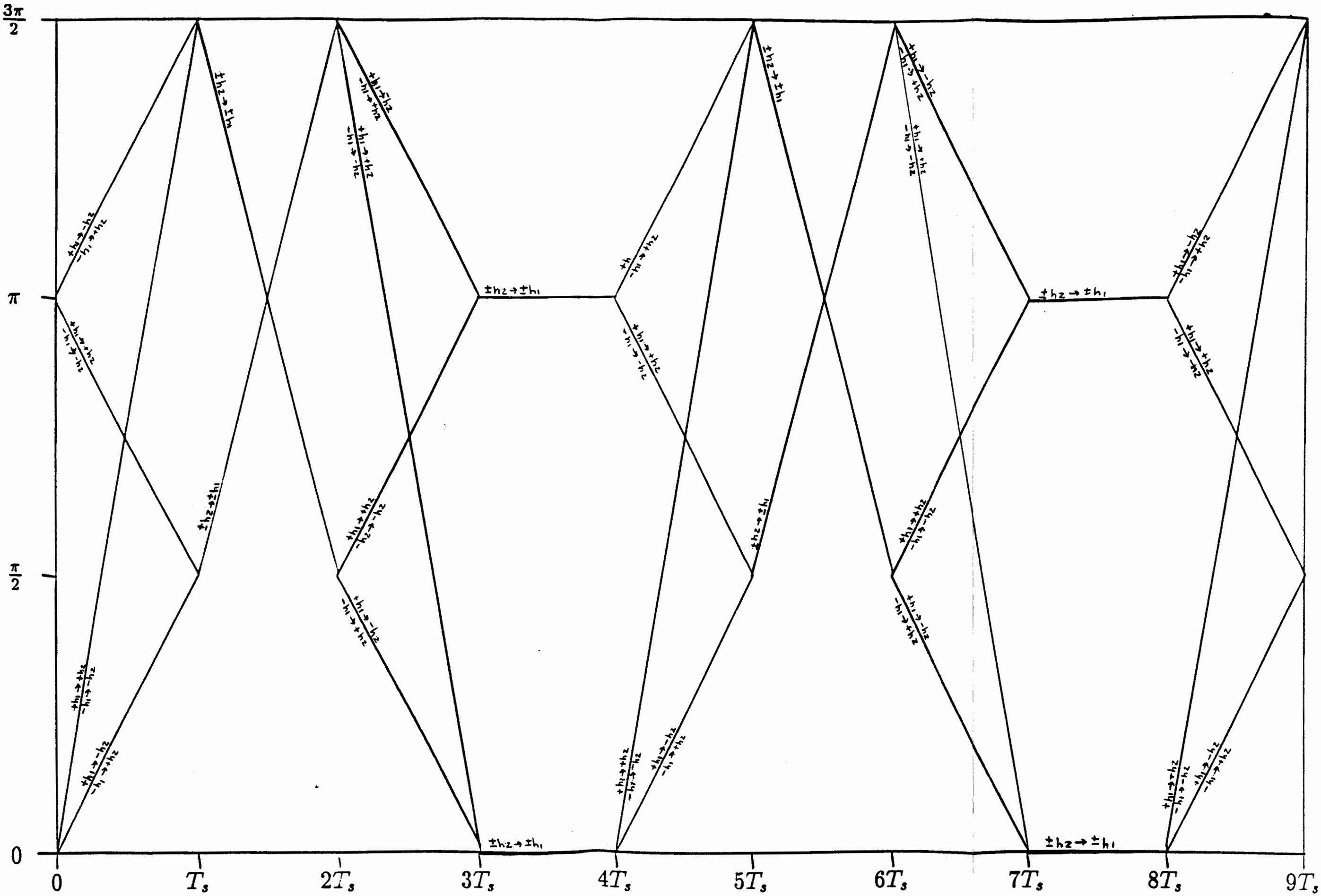

Figure 19 The multi-oscillator phase trellis for the 2-h set $\{\frac{1}{4}, \frac{3}{4}\}$